POLITECNICO DI TORINO

Master's Degree in Physics of Complex Systems

Master's Degree Thesis

A computational study of visual evoked potentials dynamics in dementia with a mesoscale brain model

Supervisors

Prof. Andrea GAMBA

Prof. Alberto MAZZONI

Candidate

Michela ROCCHETTI

A.A 2023-2024

Table of Contents

Chapter 1

Overview

1.1 Introduction

Alzheimer's disease is one of the leading causes of dementia in the elderly worldwide [1]. The disease is associated with a variety of different symptoms, such as visual, sensory and motor impairments, which are already present in early stages of the disease [2], prodromal Alzheimer's disease (pAD), but some of them are also common to other forms of dementia and to ageing.Classical diagnostic tools are not sufficient to provide answers about the evolution and the nature of the disease, due to its long course and the complexity of the related symptomatology. Consequently, over the last decade in particular, computational methods have been developed to provide reliable and affordable ways to map complex brain dynamics. In particular, much emphasis has been placed on the development of tools capable of describing brain activity using mathematical models of neural structures such as the cortex [3].Among these tools, the EU has funded the Human Brain Project, which has resulted in the development of the "The Virtual Brain" (TVB) platform, the computational tool I have used in this thesis. TVB is a powerful tool for simulating the human brain [4], providing both computational tools and standard (and healthy) brain models that can be used as benchmarks or comparisons for further studies. The human brain is modelled in the TVB framework as a weighted network of regions connected in two main clusters (one per hemisphere). Each region is composed of interacting neural subpopulations that approximate the complex short-range dynamics of cortical neurons.
In this thesis, TVB provided the model of the healthy brain and the model of the visual stimulus, and then studied the response of the network to it, modelled as a pulse train in the input to the visual cortex.
This analysis was carried out in healthy aging and in conditions of self-perceived cognitive decline [5], called Subjective Cognitive Decline (SCD), and Mild Cognitive

Impairment (MCI), a condition in which there is a loss of memory and cognitive ability but without a diagnosis of dementia. [6].

1.2 Highlights

The primary objective of this thesis is to replicate the findings derived from an experimental configuration. Specifically, the aim is to replicate the dynamics of a visual evoked potential (VEP), which constitutes an electrophysiological response triggered by a visual stimulus. The overarching goal is to observe the progression of the disease by analysing EEG data.
The simulation part involved generating simulated electrical signals from a simulated brain structure and then fitting the results to the experimental results. The simulations of brain structure and electrophysiological signals were performed using The Virtual Brain (TVB) software, which allows model-based inference of neurophysiological behaviour, reproduces brain dynamics and generates simulated brain signals such as EEG and brain imaging techniques, i.e. functional MRI and MEG.[7, 8], (more about it in section 4).

In the experiment, individuals belonging to three distinct categories (controls (CTR), Subjective Cognitive Decline (SCD), and Mild Cognitive Impairment (MCI)) were tasked with performing a visual attention task. During this task, various geometric figures were presented, and the corresponding electrophysiological responses to these stimuli, known as event-related potentials (ERPs), were recorded. The categorisation of individuals into these three classes is based on existing literature. Specifically, SCD subjects are characterised by subjective cognitive impairment associated with ageing,wherein the manifested issues do not align with a specific diagnosis and do not significantly impact their daily functioning. On the other hand, MCI subjects exhibit cognitive impairment that affects their daily lives, albeit without a definitive diagnosis of dementia. It is noteworthy that over 50% of individuals with MCI progress to develop Alzheimer's disease or other forms of dementia in subsequent years [9]. Therefore, establishing a clear differentiation between these cases is particularly valuable for diagnostic purposes.
The analysis of EEG data, coming from channels in correspondence with the visual cortex, revealed alterations in visual evoked potentials (VEPs) which are nonlinear with the worsening of the cases considered. To be specific, the negative N100 component of the evoked potential, having its minimum after 80-120 ms from the onset of the stimuli, was found to be more pronounced in the CTR case but less pronounced in SCD compared to in MCI. However, the causal mechanism of this behaviour at network level is still unclear.
To investigate further, a phenomenological mescoscale brain model was used, aiming

in reproduce, from the simulated brain structure, the electrophysiological behaviour observed analytically. To do so, The Virtual Brain platform was used, providing a whole structure of the cortex and permitting changes in model parameters in order to simulate pathological conditions.
The whole brain structure, in this thesis, is depicted by 76 nodes, each representing a brain region and described by a set of stochastic differential equations (SDE) [8].The solution of each SDE is achieved by the Euler Stochastic method with a time step of 0.1 ms, and constitutes the behaviour of each of the neural subpopulations that are illustrated in each node. The outcome of one region is then injected as input into the set of SDEs of another region by means of a coupling function. The connection between different regions is described by a connectivity matrix, modelling the human connectome by assigning a tract length and a connectivity weight to each region of the brain. The solutions of the SDEs represent the average population activity in each region and need to be processed in order to obtain the EEG outcome.
After fitting the dynamics of VEPs in the simulation presented here, a continuous progression of dementia was analysed, considering cases between those three considered for modelling to see the entire dynamics with structural degeneration of the connectome and neural mass dynamics, to see if biomarkers or phase transitions were present.

Chapter 2

Alzheimer's disease

Alzheimer's disease is a serious neurodegenerative pathology that can permanently alter the quality of life of patients. Being a geriatric pathology, the risk increases with age and it affects over 30 million people worldwide with a survival expectancy that ranges from 3 to 9 years.[10]. However, the pattern of the disease is not the same in all patients.

Because of its later onset and slow progression, Alzheimer's becomes a true social disease, as the patient becomes totally dependent on carers, usually close family members, in the later stages of the disease.
Pre-mortem diagnosis relies on behavioural and cognitive assessments to look for signs usually associated with Alzheimer's disease. Brain imaging techniques are also used to look for biomarkers often associated with the disease, but these are far from conclusive proof of Alzheimer's. It is known that Alzheimer's is a genetic disease, so most cases are due to genomic abnormalities, but other factors may have an impact on the aetiology of the disease, including lifestyle, diet, and education [11]. These factors may increase the predisposition to the disease.

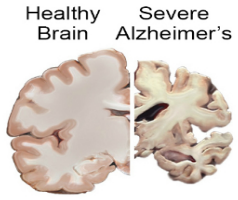

Figure 2.1: Healthy brain vs. Alzheimer's brain from www.nia.nih.gov

There are some therapeutic approaches, such as antagonists of N-methyl-D-aspartame (NMDA), e.g. memantine [12, 13], or acetylcholinesterase inhibitors [14, 15] (e.g. donepezil), but these only help with symptoms and/or slowing the spread of the disease. (e.g. donepezil), but these drugs are only useful for relieving symptoms and/or slowing the spread of the disease. Although there are clues as to the genesis and risk factors of the disease, there is still no known cure and no mechanism that can be definitively linked to the manifestations of Alzheimer's disease. A major problem is the diversity of symptoms associated with the disease and the

difficulty of distinguishing between different forms of dementia. The latter tends to be similar in both symptomatology and phenotypic manifestations, such as brain atrophy and levels of misfolded proteins in the central nervous system (CNS). In fact, one of the most important features leading to the manifestation of Alzheimer's disease is the formation of amyloid-beta plaques in certain regions of the brain [16]. Amyloid-beta is a protein that is ubiquitous in the brain and has multiple functions, such as regulating cholesterol and acting as a protein transcription factor and memory regulator [17, 18].In the brain affected by Alzheimer's disease, these proteins undergo a process of misfolding and form aggregates that can disrupt the normal functioning of brain regions, particularly by affecting the population of inhibitory neurons. As a result, these neurons function at a reduced rate compared to their functionality in a healthy brain [19]. In later stages of the disease, the accumulation of Aβ plaques is mostly intraneuronal, impairing normal synaptic functions [20] and leading to changes in the anatomical structure of the brain, with atrophy of cortical and subcortical regions. An abnormal accumulation of this protein can promote the excitability of pyramidal cells in the anterior cingulate cortex (ACC) [19], which plays a preeminent role in attention and memory, and can disrupt the activity of inhibitory/excitatory (IE) neurons, leading to cognitive decline [21]. This imbalance appears to cause a general hyperexcitability throughout the brain structure [22], resulting in excessive neuronal activity leading to neurodegeneration [23].

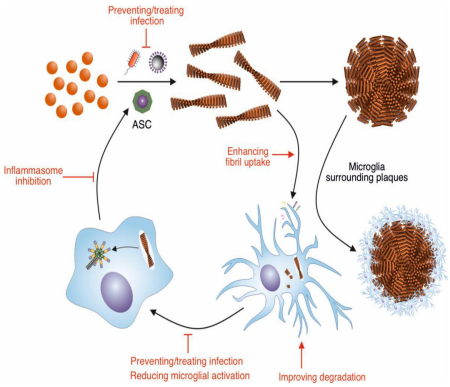

Figure 2.2: Amyloid plaque formation from [24]

The hypothesis that Alzheimer's disease is caused by the deposition of Abeta is called the amyloid hypothesis. The misfolding of Abeta is caused by enzymatic precursors that cooperate in a process in which segments of the protein are cut, but eventually end up forming clumps: the latter harm the structure and the good functioning of the brain. In fact, the deposition of Abeta leads to a behavioural change in the network, disrupting the calcium ion homeostasis of the cell and inducing inflammation in the areas involved. The neuroinflammation caused by Abeta affects long-range connectivity, leading to its loss [25]. Amyloid plaques also affect inhibitory synapses of fast spiking interneurons, which are the most common type of inhibitory cells found in the CNS [19].

Other hypotheses seem to link the presence of misfolded tau protein with the onset of the disease [27].Tau is a microtubule-associated protein (MAP) in the

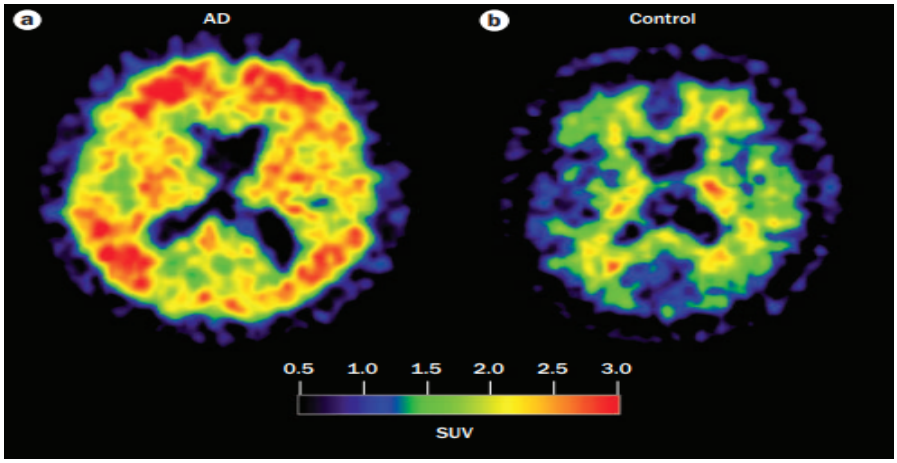

Figure 2.3: PET showing Aβ in AD brain vs. healthy brain from [26]

brain [28]: in healthy conditions, it has the role of supporting the formation of neuronal microtubules. Under pathological conditions, tau proteins can assemble into insoluble aggregates due to hyperphosphorylation, leading to synaptic dysfunction and neuronal death [28]. The diseases associated with this abnormal behaviour are collectively referred to as tauopathies[28, 27]: these include neurodegenerative diseases such as Alzheimer's disease, but also other types of dementia, e.g. Lewy body dementia, frontotemporal dementia.

When discussing AD, the tau protein's role is that it loses the ability to bind to microtubules, which promotes misfolding of the protein structure, resulting in the formation of fibrillary structures in neurons [29]. These abnormalities cause a loss of long-range connectivity through axonal damage, so the phenomenology is similar to that of Abeta. Both Abeta and tau oligomers can be the cause of Alzheimer's disease, and this is referred to as the "Abeta/Tau hypothesis". However, although these two protein aggregates can be efficiently detected with non-invasive scans, they are not adequate for diagnosing Alzheimer's disease because they are general biomarkers for various types of dementia, which make diagnosis challenging. At present, the only certain test to assess whether a patient has Alzheimer's is post-mortem examination, and post-mortem observations

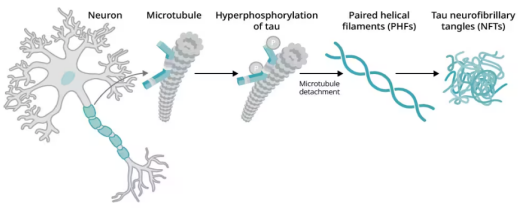

Figure 2.4: NFT formation

indicate that up to 65-70% of Alzheimer's patients have co-morbidity with at least one other form of dementia.

2.1 Staging classification

An important problem in the study of Alzheimer's disease is the difficulty in distinguishing the different stages of the disease. Before a clear diagnosis, patients present signs of cognitive deficiency in various tasks, which is known as Mild Cognitive Impairment (MCI) [30]. Prodromal signs of the disease may be present even earlier: in fact, patients may perceive a decline in cognitive function without clinical evidence, which is called Subjective Cognitive Decline (SCD). These conditions are both considered prodromal forms of Alzheimer's disease, but the transition from SCD to Alzheimer's disease and from MCI to Alzheimer's disease are not unambiguous and are based purely on observational parameters. Furthermore, MCI and SCD patients do not necessarily go on to develop Alzheimer's disease, and there is no universal method of establishing a transition probability.
Because of the difficulties in making a definitive diagnosis and distinguishing different stages of AD, it is easier to distinguish between stages of the disease if the progression of Alzheimer's is viewed as a manifestation of the spread of Abeta/tau within the brain structure, which can be observed in medical scans. The most widely used convention in this Abeta/tau hypothesis is given by the so-called Braak stages [31], which schematise the progression of AD by associating a certain degree of Abeta (tau) deposition with a stage of cognitive degeneration and are different for Abeta and tau deposition. For the latter, there are six different phases divided into three groups, which are:

1. **Braak stages I, II**: Tau deposition in the transenthorinal cortex,with mild involvement of the hippocampus no evident symptomatology;

2. **Braak stages III, IV**: Oligomers are found also in the limbic system and more massively in the hippocampus. In this stage, the patient is now showing signs of mild cognitive impairment i.e. difficulties at performing memory tasks.

3. **Braak stage V, VI**: Misfolded Tau proteins are now widely detected throughout the brain, with higher concentration in regions initially affected. This presence often coincides with the onset of classic dementia symptoms such as disorientation, depression, irritability, and amnesia. It is possible that this phenomenon may have connections to other forms of dementia or perhaps could be a consequence of the natural aging process.

About Abeta, Braak stages are tree,are denoted by letters A,B and C and share similar symptomatology with Tau Braak stages:

1. **Amyloid stage A**: Misfolded Abeta deposits of low density are found in particular in frontal,temporal and occipital cortex;

2. **Amyloid stage B**: Deposits attack ulterior regions: hippocampus and gyrus parahippocampalis, amygdala, posterior and anterior insula, subgenual and retrosplenial cingulum, ventrolateral prefrontal cortex;

3. **Amyloid stage C**: Global dissemination of abeta deposits.

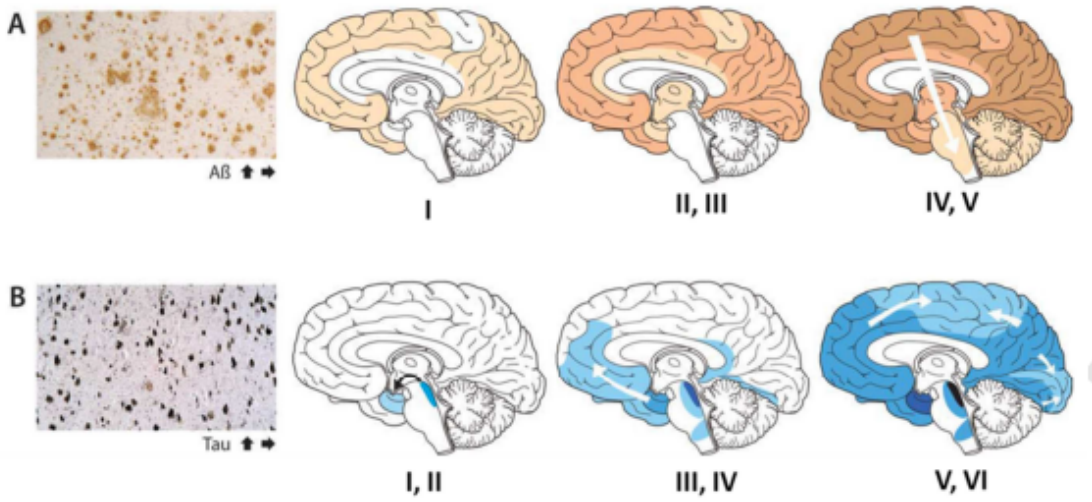

Figure 2.5: Braak staging spatiotemporal evolution from [**jouanne**]. Image **A** describes the progression in Aβ deposit. Image **B** shows the diffusion of neurofibrillary tangles (NFTs) of Tau.

The transition from MCI or SCD to AD is somewhat unclear. In the following, a more detailed description of the presented conditions is given, in order to gain insight with the main objective of the thesis.

2.1.1 Subjective cognitive decline

Subjective cognitive decline (SCD) is one of the first stages of cognitive impairment in older people who experience age-related cognitive decline in a completely subjective way: the problems they experience aren't related to a specific diagnosis and, most importantly, don't affect their daily lives. However, they do show unimpaired performance on cognitive tests, and this may be a primary symptomatic manifestation of Alzheimer's disease. The choice of the term SCD refers to the self-perception of cognitive performance, which is completely separate from cognitive test performance. Furthermore, the term refers to the cognitive domain. In fact, in pre-AD

condition, before memory impairment, people experience some other decline in other domains of cognition such as executive function, attention, language and visuospatial function[32]. Obviously, different levels of severity can be assessed in this condition. The individual may experience some impairment, but this may be opposite to their cognitive level. Conversely, there may also be cases where the SCD condition may be followed by a more severe decline in cognitive functions. There may also be an association between depression, anxiety, personality traits, or other comorbidities with SCD [33, 32]. This setting is particularly heterogeneous, and a percentage of people who present this type of cognitive impairment may improve their condition over time or remain stable. Others may instead develop Alzheimer's disease or other types of dementia, so it will be essential to distinguish these two pools of individuals in SCD condition in order to promptly individualise the disease and find adequate cures.

2.1.2 Mild cognitive impairment

Another stage of cognitive decline that may lead to Alzheimer's disease is mild cognitive impairment (MCI), which is a stage between normal ageing and Alzheimer's disease, just after SCD. Patients with MCI have some cognitive complaints that do not interfere with their activities of daily life, but that are detectable with cognitive tests [2]. In addition, these individuals have a risk of developing dementia of between 10 and 15 percent per year [34]. Some criteria for MCI can be outlined: firstly, there should be a change in the person's previous level of cognition, then there should be evidence of reduced performance in one or more cognitive domains, i.e. memory, visuospatial skills, attention, language. A person with MCI might have problems performing complex functional tasks, such as paying bills or preparing a meal, taking more time or making some mistakes. However, they will generally still be able to maintain their independence and these changes will not affect their social functioning. In general, episodic memory impairment is seen in MCI patients who go on to develop Alzheimer's disease [35]. Additionally, MCI patients have a moderate number of neuritic plaques and neurofibrillary tangles (NFTs) in the limbic system, corresponding to Braak stage III or IV [2]. The degree of cognitive impairment can be assessed using cognitive tests, the scores of which in individuals with MCI are 1 to 1.5 standard deviations below the mean for their age and education. Other cognitive domains are also evaluated, including reasoning, problem-solving, verbal fluency, and visuospatial ability. This is achieved through clinical tests such as the Boston Naming Test (language), digit span forward (attention), or figure copying (spatial ability) [35].

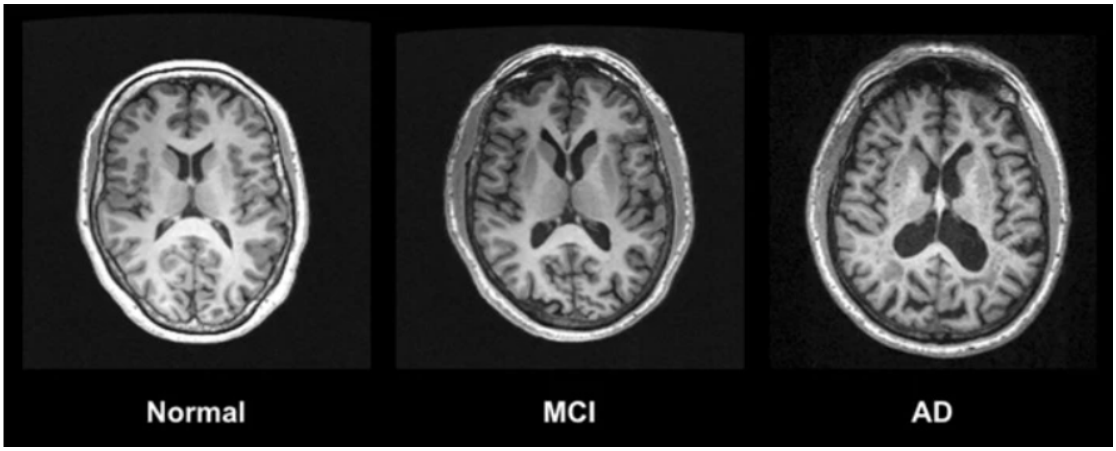

Figure 2.6: MRI scan: MRI imaging using MPRAGE (Magnetization Prepared Rapid Gradient Echo) sequence on healthy control, MCI patients and AD. It is shown a progressive reduction of grey matter (GM) volume from HC to AD. Image taken from [36]

Chapter 3

Electroencephalography and brain signal detection

Detecting brain signals can be a difficult task because the brain is a complex organ with many layers and structures, but there are many ways to approach the task. For example, detection methods such as local field potentials (LFPs) are remarkably difficult and require the insertion of electrodes deep into the brain to obtain a signal; others, such as magnetoelectroenphalography (MEG), necessitate costly and complex machines to perform.
Electroencephalogram (EEG) is one of the most useful and straightforward methods of detecting brain signals from the cortex and is a record of the brain's spontaneous electrical activity, recorded from surface electrodes placed on the scalp. Being non-invasive and affordable, it is one of the most usual and dependable neurological tests. The main idea behind the EEG is that, given the electrical nature of brain activity, we can detect it by placing electrodes as close as possible to the source of the electrical signal and thus to the brain regions involved. Sensors are attached to the patient's scalp and the signal from the underlying regions are recorded over time, and a time series of the recorded signals is displayed at the end.

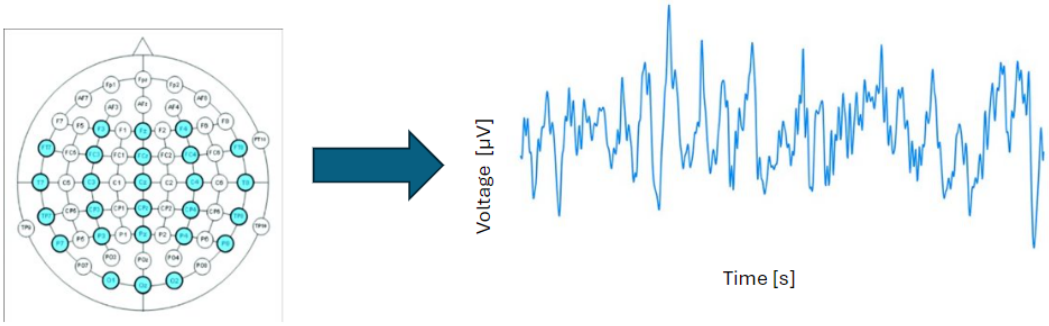

Figure 3.1: EEG processing: signal is detected from electrodes positioned on the scalp

3.1 EEG

Electroencephalogram (EEG) is a method of recording the electrical signal produced by the activity of brain cells, which is related to changes in the resting membrane potential inside the cell, which is negative with respect to the extracellular space [37]. The sum of the postsynaptic potentials (PSP) generated by millions of pyramidal cells gives rise to the recorded current [38].
Indeed, synapses located at the dendrites of neurons allow the transmission of neural activity to neighboring cells through neurotransmitters released by presynaptic cells. However, inputs can also be received in pyramidal cells by interneurons activated via thalamocortical or corticocortical fibers [37]. From these synapses, activity is transmitted to the postsynaptic cell through neurotransmitters originating from presynaptic cells. Depending on the type of neurotransmitter involved, synapses are classified as inhibitory or excitatory, and the postsynaptic potential is subsequently transmitted to other dendrites. Specifically, excitatory and inhibitory potentials are generated at the postsynaptic membrane and reach the soma via the dendrites.

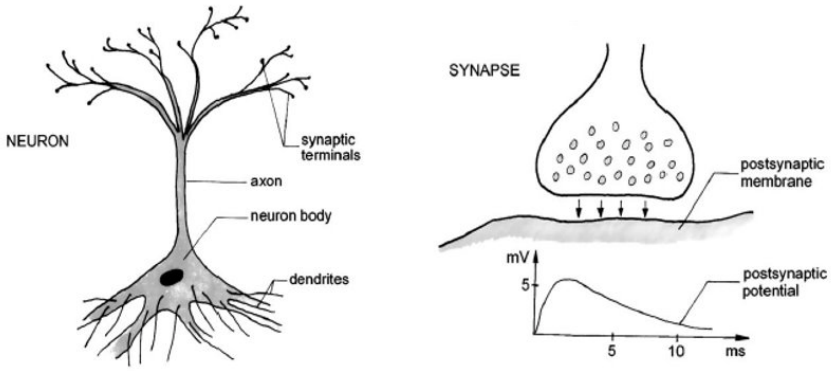

Figure 3.2: Anatomy of the neuron and synapse: Starting from the left. Neuron:i) dendrides, that propagates the signal received from other cells to the soma, ii) the neuron body, or soma, iii) the axon, conducting the action potential from the firing neuron to other cells, iv) synaptic or axon terminals, synapses are found at their end. Connection synapse- postsynaptic membrane: the action potential arrives at the synapse and there a chemical substance called transmitter is released, causing a change in the permeability of the post synaptic membrane of the following neuron, causing ions to traverse and a potential difference. If Na_+ ions are entering, there is less negativity in the neuron and this cause an excitatory postsynaptic potential (EPSP). On the contrary, when the neuron is more negative i.e influx of K_- ions, a inhibitory postsynaptic potential (IPSP) is generated [39].Image from [39]

The postsynaptic signal originates not only from a single neuron, but rather from multiple signals arriving from various dendrites. These signals undergo integration, and if the integrated signal causes depolarization at the initial axon segment surpassing a certain threshold, it triggers the generation of an action potential that propagates to the synaptic terminal. Cortical pyramidal cells, a type of neuron possessing two dendritic trees, also receive synaptic inputs. These cells are activated by both thalamocortical and cortical fibers. The connection between thalamocortical afferents and pyramidal cells is more prominent in deeper cortical layers, whereas corticocortical afferents synapse with pyramidal cells across all cortical layers.

The origin of rhythmic EEG activity is still debated: it can be caused by single

cells or by oscillating neural networks. However, it is established that the rhythms of the EEG are given by networks of inhibitory and excitatory neurons connected in feedback loops, and the oscillation frequency depends on the membrane potential of the individual neuron and on the strength of synaptic interactions [39]. Nevertheless, five different rhythms have been identified in EEG, those are:

- **Delta rhythm** (0.5-4 Hz): predominant in deep sleep situations. Here the waves have coherent large amplitude (generally 75-200 μV) all over the scalp.
- **Theta rhythm** (4-8 Hz): rare in humans, may occur in some emotive state and can be connected to a slowing of alpha rhythm in some pathology.
- **Alpha rhythm** (8-13 Hz): mostly common in fully awake state and are best observable in the posterior region of the head, when the subject is resting with close eyes. They are attenuated,evenly blocked, by attention and visual mental effort.
- **Beta rhythm** (13-30 Hz): present in states of focus and alertness.
- **Gamma rhythm** ($>$ 30 Hz): related to the processing of information (i.e a sensory stimulus) and the onset of voluntary movements. [39]

Despite its limitations, EEG is still one of the most used and applied tool due to its reliability and effectiveness as well as its reduced cost, with different application in many fields ranging from medicine and diagnostic to linguistic. It has been shown to be effective in supporting diagnosis of diseases such as brain tumour [40], stroke [41], epilepsy [42], brain injury [43], sleep disorders [44], and, especially in recent years, it is also gaining momentum for studies of autism and developmental disorders (such as ADHD) [45], as well as neurodegenerative diseases or psychiatric disorders. Thus, the study of EEGs, their origin and behaviour, could lead to an expansion of their use in diagnosing brain disorders as well as predicting treatment [38].

3.2 ERPs and VEPs

When recording signals from the scalp, two main components can be distinguished: Event-Related Potentials (ERPs) and Evoked Potentials (EP). Both are elicited in response to an external stimulus and are highly valuable for their ability to offer insights into the dynamic cognitive processes of the brain [46] in a non-invasive and straightforward manner.

ERPs are minute voltage fluctuations generated in the brain following the detection of an external event or stimulus [47]. The waveform of an ERP comprises

a sequence of wavelike components, characterized by their polarity and temporal occurrence [46]. Additionally, the polarities of these waveform components are denoted by the letter P for positive and N for negative, followed by a number indicating the milliseconds after stimulus onset at which the polarity change occurs. In humans, ERPs can arise from various types of events, including motor events, cognitive processes, or sensory stimuli. Therefore, they can be categorized into three groups based on their generation mechanisms [46]:

- Sensory: Sensory ERPs can be triggered by an external stimulus in any sensory modality and detected through electrodes positioned within sensory brain structures,on the overlying scalp or on the surfaces of sensory cortices.
- Motor: those ERPs are extracted from noise given by a movement-related event by doing an ensemble average with respect to it . The characteristics of motor ERP components depends on the subject's internal state and not on the stimulus' components.
- Cognitive: generated to cognitive processes of the brain.

The various components of an ERP signal can also be classified into two categories. The first category comprises "sensory" or "exogenous" waves, which peak within 100 ms after the stimulus onset. The second category includes "endogenous" ERPs, generated at a later stage, reflecting how the stimulus is processed by the subject [48].

Evoked potentials are changes in the response of the nervous system when elicited by an external stimulus [49].

A specific type of EP that is of interest in this thesis is the visual evoked potential (VEP), which refers to a distinct electrical signal recorded on the scalp during electroencephalography following the presentation of a brief visual stimulus, and subsequently extracted via signal averaging [50]. Typically, the electrode used to record the signal is placed on the back of the head, along the midline of the occipital scalp. VEPs are employed to assess the integrity of the occipital cortex, the pathways to the visual cortex of the brain, and the optic nerves.

Abnormalities affecting the visual pathway—which includes the eye, optic nerve, optic chiasm, optic tract, optic radiation, and cerebral cortex [51]—or the visual cortex may manifest as deviations in the VEP [52]. Examples of conditions leading to VEP abnormalities include optic neuritis due to demyelination, stroke, tumors compressing the optic pathways, and retinal diseases, particularly macular degeneration.

Although the neural generators of VEPs are not yet fully understood, it is known that the primary visual cortex V1 is a significant contributor to their generation [53].

The analysis of VEPs typically occurs within a timeframe of 200-500 ms following the stimulus onset, during which various components can be distinguished. These components include a negative peak known as N1 (or N100), occurring around 70 ms, followed by a positive peak (P1) at approximately 100 ms, and subsequently another negative peak (N2). Common visual stimuli used to evoke VEPs include LED flashes and rotating checkerboard patterns, often accompanied by a red fixation point. The latter stimulus is preferred due to its consistency within individuals, facilitating comparisons across subjects.

There may be correlations between different VEP responses and Alzheimer's disease. For instance, patients with probable Alzheimer's disease tend to exhibit delayed responses in the P2 component elicited by flash stimuli, while significant latency changes in the P2-P100 components are observed in cases of moderate to advanced dementia [54]. However, changes in the N1 component have not been reported.

In this study, the focus is on the visual evoked potential and its variations under different conditions. Therefore, the analysis concentrates on the initial segment of the signal recording, spanning from 0 to 200 ms, where the immediate response to the stimulus is evident. This segment is obtained by averaging signals from the EEG, specifically from five dipoles positioned on the occipital scalp region, namely channels O1, O2, OZ, P01, and P02.

Chapter 4

Methods

4.1 Theory of Neural Mass Model

The brain, characterized by its complex behavior across various length and time scales [55], necessitates a mesoscopic approximation to simulate large-scale brain network models and their macroscopic spatio-temporal dynamics [4, 56, 57]. In this approximation, pools of cortical neurons sharing similar characteristics aggregate to form regions known as cortical columns or macrocolumns [58]. Neurons within the same macrocolumn tend to respond synchronously to similar inputs. Specifically, sensory neurons exhibiting similar responses (or, in the case of sensory neurons, similar receptive fields [59]) are organized into cylindrical structures perpendicular to the brain surface [60].

Figure 4.1: Microcolumn and pyramidal neurons. Adapted from [61]

A pool of cortical columns constitutes a region of the cortex, with each column comprised of microcolumns [62]—smaller functional units consisting of strongly interconnected neurons. The temporal behavior of these structures is elucidated by a system of equations, which serves as a mathematical translation of ensembles of neurons.

The aforementioned structures are characterized by models developed using a mass-action approach. Here, clusters of neurons sharing similar characteristics form a neural mass (NM) [63]. In light of the brief biological description mentioned earlier, interactions between neurons within the same region or column are represented by interactions between population activities [4]. Neural masses vary in size depending on the model considered, ranging from a

few neurons or microcolumns to an entire cortical region. An assembly of these NM units constitutes a brain network model (BNM), which has been utilized to simulate realistic neural behavior, ranging from scenarios of resting-state activity to the execution of minor tasks [64].

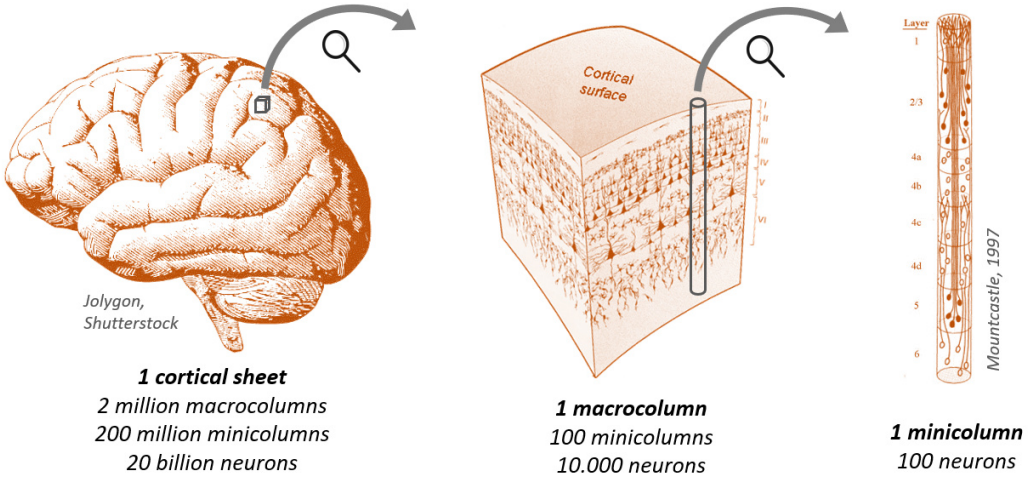

Figure 4.2: Brain parcellation: representation of brain parcellation from cortex to microcolumns. Drawing by Jolygon,Shutterstock

4.1.1 Mathematical description of neural mass model

The connectivity of the network is hierarchical, the most basic of the elements is a single variable equation as:

$$D(\frac{d}{dt})w(t) = \epsilon(t) - \alpha(x) \tag{4.1}$$

this,describes the temporal evolution of a single state variable y, with $D(\frac{d}{dt})$ as a temporal differential operator [8].
The next level of hierarchy is to describe the behaviour of a neural mass, which can be done with the Langevin's equation:

$$\mathbf{D}(\frac{d}{dt})w(t) = \mathbf{E}(t) - \mathbf{A}(x(t)) \tag{4.2}$$

Where **E**(t) is the matrix of external inputs. **A**(t) is the matrix for the relations of state variables in the neural masses.Here, to describe an ensemble of single neural masses, thus additional degrees of freedom are present and thus more than one state-variable: one describe the neural activity,the other can describe external processes occurring at a slower time scale. Moving to a local network of neural masses, the evolution is:

$$P(\frac{d}{dt})W(t) = -\Lambda(W(t)) + Z[\Xi(t) + U_{\nu=0} \circ V_{\nu=0}\Gamma W(t)] \tag{4.3}$$

P($\frac{d}{dt}$) Where P(d/dt) denotes a differential operator that maps W(t) into their derivatives. Γ is a matrix representing external inputs, like noise or a stimulus. Λ is a matrix considering the action of a state operator on each neural mass in the vector W(t) . $V_{\nu=0}$ is the matrix of interaction between neural masses and is weighted by the matrix $V_{\nu=0}$.The terms Z and Γ are coupling functions, transforming the activity of the NMs' state variables. The $\circ$ is the Shur-Hadamard product between matrices. Lastly, the ultimate level is an equation for the general for a brain network model:

$$\hat{P}(\frac{d}{dt})\hat{W}(t) = -\hat{\Lambda}(\hat{W}(t)) + Z[\hat{\Xi} + \sum_{\nu=0}^{2} U_\nu \circ V_\nu \Gamma_\nu [W(t - K_\nu C_\nu)^{-1}]] \tag{4.4}$$

Where now K_ν is a matrix of distance between nodes and C_ν is the propagation speed of brain signals. The index ν goes from 0 to 2. When is 0, the quantities are related a single or a local network of NMs When $\nu = 1$, the interaction is between local networks of NMs,those are coupled in a geometrical representation of the cortex by means of local connectivity kernels, functions meant to take into account the morphology of cortical layers, finally. When $\nu = 2$, the equations describe long range interaction between different local networks.

Scale	ν	Representation
State variable	-	$D\left(\frac{d}{dt}\right) w(t) = \epsilon(t) - \alpha(\phi(t))$
Neural mass	-	$D\left(\frac{d}{dt}\right) W(t) = E(t) - A(\Phi(t))$
Neural mass model	0	$P\left(\frac{d}{dt}\right) W(t) = -\Lambda(W(t)) + Z\left[\Xi(t) + U_{\nu=0} \circ V_{\nu=0}\Gamma W(t)\right]$
Brain network model	0,1,2	$\hat{P}\left(\frac{d}{dt}\right) \hat{W}(t) = -\hat{\Lambda}(\hat{W}(t)) + Z\left[\hat{\Xi} + \sum_{\nu=0}^{2} U_\nu \circ V_\nu \Gamma_\nu [W(t - K_\nu C_\nu)^{-1}]\right]$

Table 4.1: BNM hierarchical structure. Respectively, in order of appearance: single variable equation, single neural mass dynamics, neural masses local network, dynamics of a discrete approximation of neural fields present on the surface of the cortex, those includes also long-range connectivity

Scale	ν	Representation
State variable	-	$D(\frac{d}{dt})w(t) = \epsilon(t) - \alpha(\phi(t))$
Neural mass	-	$D(\frac{d}{dt})W(t) = E(t) - A(\Phi(t))$
Neural mass model	0	$P(\frac{d}{dt})W(t) = -\Lambda(W(t)) + Z[\Xi(t) + U_{\nu=0} \circ V_{\nu=0}\Gamma W(t)]$
Brain network model	0,1,2	$\hat{P}(\frac{d}{dt})\hat{W}(t) = -\hat{\Lambda}(\hat{W}(t)) + Z[\hat{\Xi} + \sum_{\nu=0}^{2} U_\nu \circ V_\nu \Gamma_\nu [W(t - K_\nu C_\nu)^{-1}]]$

Table 4.2: BNM hierarchical structure. Respectively, in order of appearance: single variable equation, single neural mass dynamics, neural masses local network, dynamics of a discrete approximation of neural fields present on the surface of the cortex, those includes also long-range connectivity

4.1.2 Jansen-Rit model

The mathematical framework utilized to simulate EEG activity is based on the model developed by Jansen and Rit [65, 66], which can represent activity both in the resting state and during the presence of an event-related potential (ERP). This model delineates the activity of three distinct neural populations: two excitatory and one inhibitory. Among the excitatory populations, the pyramidal neurons receive inhibitory and excitatory feedback from interneurons, along with an external excitatory input originating from neighboring cortical and subcortical structures [65, 8]. This external input can be modeled using the same formalism as other components or as an external stochastic input. It's important to note that only pyramidal cells among the excitatory interneurons are capable of generating a signal detectable by EEG.

In the right subfigure 5.9, the incoming input p(t), depicted as a mean firing rate (s^{-1}), is coupled to a Post Synaptic Potential (PSP) by means of a function h(t) with an index specific for the type of neuron we're considering. These functions describe linear stationary systems and can be written as a convolution with a response function:

$$h(t) = \begin{cases} Aate^{-at}, & \text{if } t \geq 0 \\ 0, & \text{if } t < 0 \end{cases} \tag{4.5}$$

or, in terms of a second order linear differential equations, as [65] :

$$\ddot{y}(t) = Aap(t) - 2a\dot{y}(t) - a^2 y(t) \tag{4.6}$$

The constants are different,depending on the nature of the population we're considering. Alpha is the maximal amplitude of the post-synaptic potential, expressed in mV; beta instead is expressed in s^{-1} and lumps together dynamic features such as delays of the synaptic transmission,which is the time constant of the membrane,

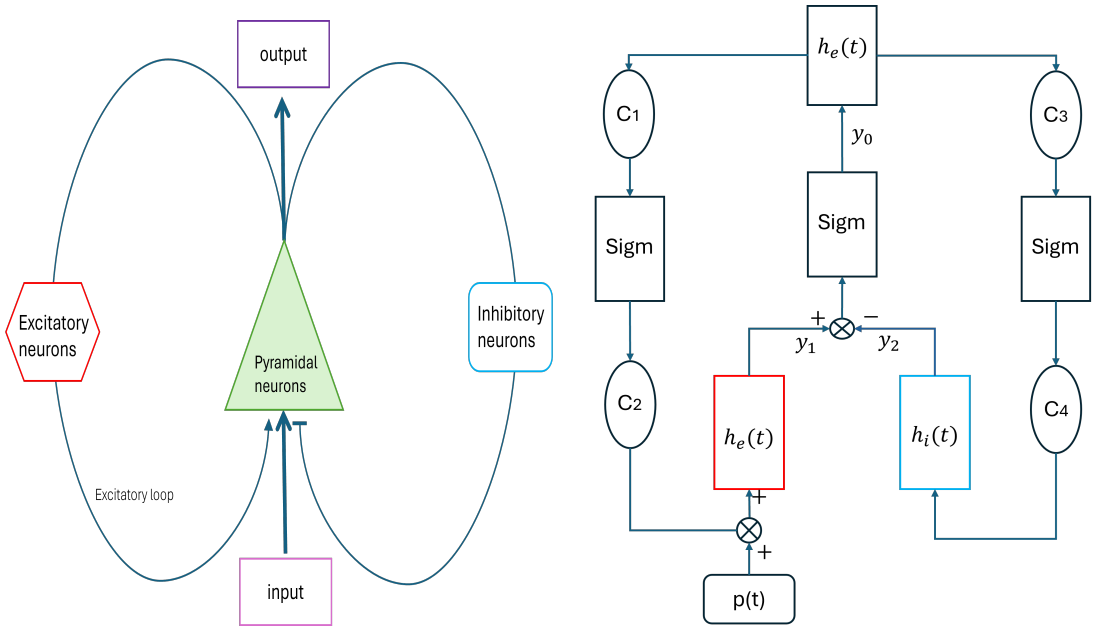

Figure 4.3: (a) simplified block diagram of feedback loop in Jansen-Rit model (b) more detailed block diagram of Jansen-Rit

and the delay in signal transmission due to the propagation along thedendritic tree. In the excitatory (inhibitory) case we have a = A, a = a (b = B, beta = b). p(t) is the input, written as a firing rate.

The Sigmoid represents the gain function that transforms the population's average membrane potential into an average firing rate of neurons.

$$Sigm(v) = \frac{v_{max}}{2}[1 + tanh\frac{r}{2}(v - v_{max})] = \frac{2v_{max}}{[1 + e^{r(v-v_0)}]} \tag{4.7}$$

The term v_{max} is the population of neuron's maximum firing rate, v_0 is the post synaptic potential (PSP) corresponding to the achieving of 50% firing rate, r is the sigmoid's slope [66] . Naming the three outputs of the system y_0,y_1,y_2,each corresponding to a PSP for a given population, and y_4, y_5, y_6 the corresponding derivatives, the following system of equations can be written:

$$\begin{cases} \frac{d}{dt}y_0(t) = y_3(t) & \frac{d}{dt}y_3(t) = AaSigm[y_1(t) - y_2(t)] - 2ay_3(t) - a^2y_0(t) \\ \frac{d}{dt}y_1(t) = y_4(t) & \frac{d}{dt}y_4(t) = Aa\{p(t) + C_2Sigm[C_1y_0(t)]\} - 2ay_4(t) - a^2y_1(t) \\ \frac{d}{dt}y_2(t) = y_5(t) & \frac{d}{dt}y_5(t) = BbC_4Sigm[C_3y_0(t)] - 2by_5(t) - b^2y_2(t) \end{cases} \tag{4.8}$$

where $C_1 ... C_4$ are the connectivity constant characterizing the interaction between each neuron type. Then, the hypothesis that the interaction between different cortical columns give rise to VEPs components was followed, here exploring two coupled columns. To do so, twice as many variables as for the single colums are needed i.e $y6, y7, y8$. To represent the delay between two columns,four additional variables are defined: $y_1 2, y_1 3, y_1 4, y_5$. The following equations are then defined:

$$\begin{cases} \frac{d}{dt}y_6(t) = y_9(t) & \frac{d}{dt}y_9(t) = A'a\,\mathrm{Sigm}[y_7(t) - y_8(t)] - 2ay_9(t) - a^2 y_6(t) \\ \frac{d}{dt}y_7(t) = y_{10}(t) & \frac{d}{dt}y_{10}(t) = A'a\{p'(t) + C_2'\,\mathrm{Sigm}[C_1' y_6(t)]\} + K_1 y_{12} - 2ay_{10}(t) - a^2 y_7(t) \\ \frac{d}{dt}y_8(t) = y_{11}(t) & \frac{d}{dt}y_{11}(t) = B'bC_4'\,\mathrm{Sigm}[C_3' y_6(t)] - 2by_{11}(t) - b^2 y_8(t) \\ \frac{d}{dt}y_{12}(t) = y_{14}(t) & \frac{d}{dt}y_{14}(t) = A'a_d\,\mathrm{Sigm}[y_1(t) - y_2(t)] - 2a_d y_{14}(t) - a^2 y_{12}(t) \\ \frac{d}{dt}y_{13}(t) = y_{15}(t) & \frac{d}{dt}y_{15}(t) = A'a_d\,\mathrm{Sigm}[y_7(t) - y_8(t)] - 2a_d y_{15}(t) - a^2 y_{13}(t) \end{cases} \tag{4.9}$$

For the delay's modeling, a linear transformation similar to the one previously defined is used, but with a longer latency:

$$h_d(t) \begin{cases} Aa_d t e^{-a} d^t & t \geq 0 \\ 0 & t < 0 \end{cases} \tag{4.10}$$

Having $a_d \approx a/3$.

Parameters	Description	Values	Measurement units
A	maximum EPSP (Excitatory post synaptic potential)	3.25	mV
B	maximum IPSP (Inhibitory post synaptic potential)	22.0	mV
a	Reciprocal of excitatory time constant	**0.107**	s^{-1}
b	Reciprocal of inhibitory time constant	0.05	s^{-1}
v_0	Voltage threshold when 50% firing rate is achieved	6.0	mV
$\nu_{\max}$	Maximum firing rate of neural population	0.0002	s^{-1}
r	Steepness of sigmoidal transfer function	0.56	mV^{-1}
J	Average number of synapses between populations	135	Number
C_1	Average probability of synaptic contacts in the feedback excitatory loop	1.0	Number
C_2	Average probability of synaptic contacts in the slow feedback excitatory loop	0.8	Number
C_3	Average probability of synaptic contacts in the feedback inhibitory loop	0.25	Number
C_4	Average probability of synaptic contacts in the slow feedback inhibitory loop	0.25	Number
$p_{\max}$	Maximum input firing rate	0.32	s^{-1}
$p_{\min}$	Minimum input firing rate	0.12	s^{-1}
μ	Mean input firing rate	0.22	s^{-1}

Table 4.3: Jansen Rit Model parameters. The values highlighted are the quantities modified that will be modified with respect to the healthy default case, in order to depict the pre AD effects in MCI. In more advanced states, connections between populations we will also be modified, due to processes of apoptosis not relevant in the early stages of the disease.

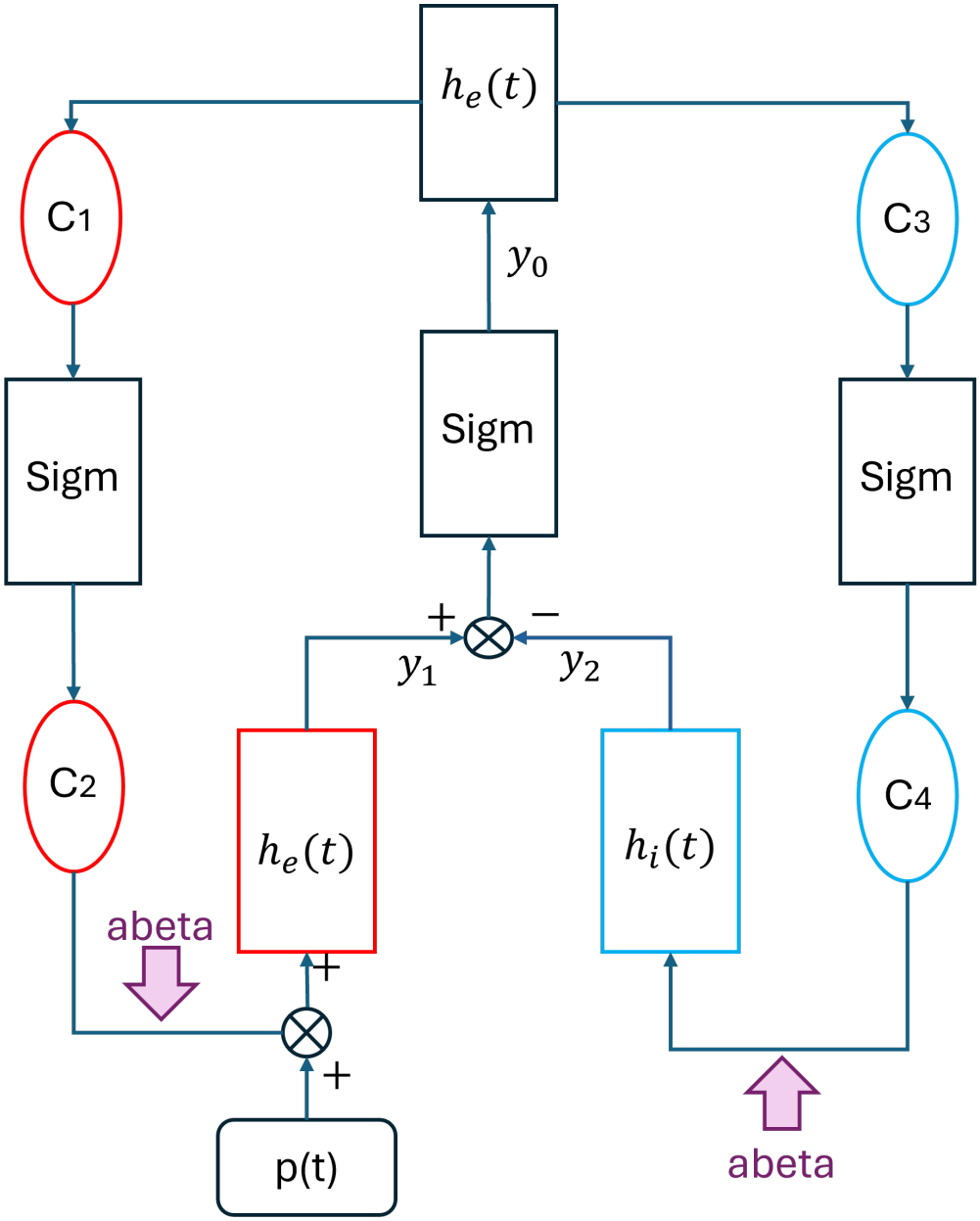

Figure 4.4: Modified block diagram of the Jansen-Rit model, with purple arrows indicating where modifications have been made.

4.2 Sarvas Model

The mathematical approximation used in order to compute the projection matrix i.e. the mapping of the local cortical activity into the mesh electrodes of simulated

EEG, takes the name of Sarvas model [67]. Here follows a brief discussion.
Let the current derived from the electrical activity in conducting biological tissue be J_i. The conductor **G** in which J_i is measured has a conductivity σ. From quasistatic approximation of the Maxwell'S equations,the electric field **E** is:

$$E = -\nabla V \tag{4.11}$$

$$J = J_i = \sigma E \tag{4.12}$$

Where **J** is the total current density , σE the total Ohmic current and V is the electric potential. Because of quasistatic approximation, $\nabla \cdot J = 0$, so substituting in the last written equation, it is :

$$\nabla \cdot (\sigma \nabla v) = \nabla \cdot J_i \tag{4.13}$$

In a region with constant conductivity

$$\Delta V = \nabla \cdot J_i / \sigma \tag{4.14}$$

If the conductor coincides with the whole space with a constant σ conductivity, this equation has solution

$$V(r) = -\frac{1}{4\pi\sigma} \int_G \frac{\nabla' \cdot J_i(r')}{|r - r'|} dv' \tag{4.15}$$

Using the identity

$$\nabla' \cdot (J_i(r_i)|r - r'|^{-1}) = |r - r'|^{-1} \nabla' \cdot J_i(r') + J_i(r') \nabla' \cdot (|r - r'|^{-1}) \tag{4.16}$$

with $\nabla' \cdot (|r - r'|^{-1}) = |r - r'|^{-3}(r - r')$ and applying the Gaussian theorem:

$$V(r) = \frac{1}{4\pi\sigma} \int_G J_i(r') \frac{r - r'}{|r - r'|} dv' \tag{4.17}$$

If the source is dipolar, with a current in a single point r_0 : $J_i(r) = \delta(r - r_0)Q$, the equation for the potential became:

$$V(r) = \frac{1}{4\pi\sigma} Q \cdot \frac{r - r'}{|r - r'|^3} \tag{4.18}$$

The latter is the approximation used by the OpenEEG software to compute the projection matrix. In the program, the head is modeled as a triple-layered mesh with conductivities that are different for each layer. At the boudaries, we need conditions with unique solution

$$V' = V" \tag{4.19}$$

$$\sigma' \partial V' / \partial n = \sigma" \partial V" / \partial n \tag{4.20}$$

4.3 The Virtual Brain

The Virtual Brain is an open-source platform for neuroinformatics, funded by the EU. Its fundamental purpose is to provide a framework for simulating neural networks, ranging from single neurons to entire brain-scale models, and to make this accessible and understandable to researchers and enthusiasts from diverse backgrounds. Within this environment, users can conduct multi-scale simulations, beginning with specific mathematical models and subsequently deducing the mechanisms underlying the generation of simulated macroscopic signals such as EEG, fMRI, and MEG [8]. One of the significant advantages of TVB as a simulation software, which also accounts for its widespread usage, is its remarkable ease of use and the flexibility of its kernel. This allows researchers to efficiently manipulate the model by adjusting external parameters or the nodes and connectivity of the network, enabling rapid modifications through an intuitive interface.

4.3.1 TVB Architecture

The two components constituting the system's architecture are a supporting interface with its graphical user interface (GUI) and a scientific computer core, accessible as a Python library.Those blocks communicate with each other via TVB-Datatypes, that will be introduced thereafter.

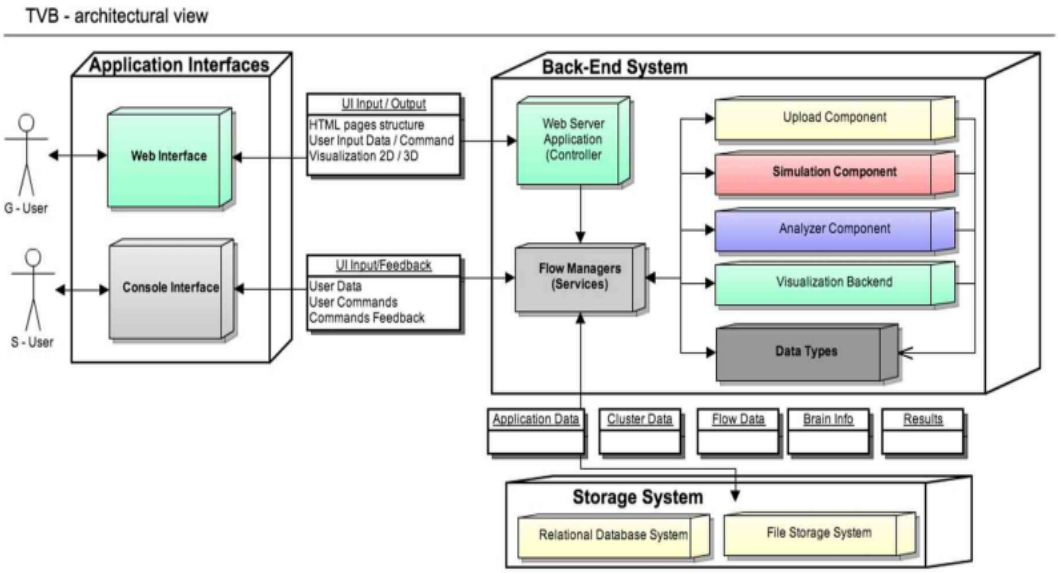

Figure 4.5: Architecture of TVB from [7]

4.3.2 TVB Framework

TVB framework is costumized to be intuitive and understandable as much as possible to researchers and people coming from various field, the distribution is thus accessible, the code is open source and is mostly written in python, with a simple GUI to allow high level simulations and analysis also to whom may not have a strong numerical and computational background.

4.3.3 TVB-Datatypes

TVB-Datatypes (TVBD) are data structures, containing data and attributes and information associated with them, and they fed directly the TVB-Simulator. They are an intermediate layer, permitting the flow and the management of data between kernel and supporting framework. For example, a TVBD is the TVB-Connectivity, which,when creating a Simulator, is a required input. At the end of the simulator's execution, other datatypes are created, as TimeSeries datatypes. [8]

4.3.4 TVB Simulator

TVB-Simulator is the operative part of the kernel. It is the simulating core of TVB, able to generate and emulate experimental real life results meshing mesoscopic models of neural dynamics with structural data [8]. Simulations are able to recreate the brain dynamics,starting from the spatial support and the brain connectivity, solving a system of coupled differential equations by numerical integration. All the entries are rapresented as classes, in modules or datatypes, and bound in a simulator class.

Connectivity

Connectivity is a class used to determine the spatial configuration of brain's regions, but also to assign conduction delays and strength between them.

Coupling

The activity of the brain propagates along the connectivity . The primary purpose of the connectivity function is that to rescale the activity depending on the model considered. Coupling class and functions are implemented in a coupling module, Sigmoidal or Linear for instance.

Model

Those are systems of differential equations, describing the activity of a given parcellation of human brain population using a mean-field approach. Various of

those population models are available on TVB, but others can be developed by the users.

Integrator

The Integrator module contains integration schemes used to solve both deterministic and stochastic differential equations.Among the available schemes implemented Euler and Heun methoad are present. Also 4-th order Runge-Kutta method is available, but only to solve ordinary differential equations.

Noise

Noise module has a crucial role for the dynamics of the brain simulation. This module is based on two classes: RandomStream, and Noise. The Noise module here enters as an additional term in stochastic integration schemes,as an Additive or Multiplicative process.

Stimulus

The stimulus module is fundamental for this thesis' developement and its attribute is used to sumulate the injection of an EM wave in one or more nodes of the network, deciding its features. The user can choose various waveforms to be injected in the desired regions and they both be deterministic or stochastic, and it is possible to recreate,in this way, life-like situations or exams.

Monitor

This class has the role of manipulate and record the simulation output while it is still running, so when the differential equations constituting the model are being integrated.The result is a a DataType TimeSeries, an array of 4 dimensions. Module class can be divided into two main categories : *low level* (raw),returning, for each time,all the simulated data, and *high level* (biophysical), which outcome concerns the simulation of realistic measurements (i.e EEG,MEG etc.). For low- level monitors, the array‘s dimensions corresponds respectively to time,state variables,space (brain regions or vertices of cortical/non cortical regions) and modes; for high level monitors, dimensions are [time,1,sensors,1].Moreover, since is our interest for this tractation, it is remarkable to enhance how the simulation of EEG signals happens.About the module simulating this specific task, and also the same holds for MEG simulation, a *ProjectionMatrix* is required: the latter maps the activity of the source ("space") to the one of the sensor ("sensors")and is generated by a software called OpenMEEG [**gramford**], corresponding to a modeling of depth electrodes signal. In Neural Mass Models implemented in TVB, the type of neural

activity,i.e firing rate,PSP etc, is depicted by one or more state variables, and they are used in the *Monitor* to derive biophysical measurement.Precisely, for the JansenrRit model, the post-synaptic potential (PSP) of pyramidal cell population is a state variable and is best suited to simulate EEG exams in presence of an external stimulus, as well as resting state EEG (rsEEG).Here, the *ProjectionMatrix* is generated by OpenEEG following the rules of the Sarvas Model [67].

Many studies have proven the reliability of The Virtual Brain as a computational tool to describe healthy brain condition. So far, TVB has been fundamental in numerous studies exploring mathematical models of various diseases, including brain tumors [68],epilepsy [69] as well as Alzheimer's disease [70]. Few steps are moving forward the characterization of prodromal stages of Alzheimer's disease and the intermediate stages that can lend to development of neurodegenerative diseases, ad Subject Cognitive Decline and Mild Cognitive Impairment conditions.

4.4 Simulations and model analysis of the disease

To simulate the SCD and MCI conditions, the Jansen-Rit model was used in the Virtual Brain. In particular, the model parameters related to the local dynamics of neuronal populations and the structural weight of the connectome. Further details will be provided later in this thesis.
The structural weight parameter, i.e. the weight assigned to each tract of the connectome, can vary from 0 to 3, and this value is used to change the weight of the connectivity matrix values.The value 1 was chosen for the SCD condition, while the value 2 was chosen for the MCI condition. In terms of dynamics, the value associated with the dynamics of the excitatory neurons is 0.1055 in SCD and 0.112 in MCI, so it's increasing; the parameter of the dynamics of the inhibitory neurons is instead decreasing, with 0.037 in SCD and 0.0257 in MCI. The three parameters take the value in the healthy state: 0.78, 0.1002 and 0.472.
These three parameters describe the dynamics of the three different networks. To describe the effect of an external visual stimulus, these parameters were also taken into account.

4.5 PREVIEW: experimental setup and results

The idea for the PREVIEW study (EVolution of SubjectIvE Cognitive Decline to Alzheimer's disease With machine learning) arose from the need to investigate biomarkers and predictors of Alzheimer's disease, mild cognitive impairment and dementia in patients with subjective cognitive decline.This is done integrating data and results coming from EEG and ERP signals with machine learning tool [71, 72,

73].

In this study, a cohort of 145 subjects was recruited, including 86 individuals meeting the criteria for Subjective Cognitive Decline (SCD), 40 with Mild Cognitive Impairment (MCI), and 19 healthy controls. All SCD participants were aged between 45 and 90 years and reported experiencing cognitive decline for a minimum of 6 months. Inclusion criteria involved a comprehensive evaluation of their clinical history and a battery of neurological and neuropsychological assessments. Specifically, participants were required to achieve a Mini Mental State Examination (MMSE) score above 24, exhibit no indications of MCI or dementia, and demonstrate normal functional abilities in daily living tasks.

Individuals meeting these criteria underwent further assessments, including detailed examination of personal and familial medical histories, as well as premorbid intelligence and personality evaluations. Additionally, screenings for depressive states were conducted. Further diagnostic evaluations involved the measurement of folic acid and vitamin B12 levels in blood samples, as well as lumbar puncture procedures to assess concentrations of Aβ, tau, and phosphorylated tau in cerebrospinal fluid (CSF) [71].

EEG data were collected from selected patients at the IRCCS Don Gnocchi (Florence, Italy) using the 64-channel Galileo-NT system, positioned according to the international 10-10 system. The signals were recorded at a sampling rate of 512 Hz, with an impedance between 7 and 10 Ω. To remove artifacts from the recorded signals, they underwent bandpass filtering at 1-45 Hz, interpolation, re-referencing, and removal of unwanted artifact components using Independent Component Analysis (ICA). Components from ERPs were epoch-aligned with their stimulus responses [72].

The experiment consists of several tasks, including a resting-state task, a 3-choice vigilance task (3CVT), and a standard image recognition task (SIR). Initially, resting-state EEG data were collected. During this phase, participants were instructed to maintain a comfortable position while EEG activity was recorded. They were prompted to keep their eyes open for a duration of 3 minutes, followed by 3 minutes with their eyes closed. This sequence was repeated twice, and for the purpose of analysis, only the EEG signals recorded during the eyes-closed condition were considered.

The ERP registration task encompasses both the 3-Choice Vigilance Test (3CVT) and the Standard Image Recognition (SIR) tasks.The 3CVT is a visual attention test involving the identification of a target shape, specifically an upward-facing

triangle, among two other distinct shapes which serve as distractors (a diamond and a downward triangle). Each shape is displayed for a duration of 200 ms. Following this presentation, participants are required to indicate whether the displayed shape corresponds to the target by pressing a left button if affirmative, and a right button otherwise. The decision-making window for this task is set at 800 ms, resulting in a total trial duration of 1000 ms. The Standard Image Recognition (SIR) task has the purpose of evaluating image recognition memory, it is composed of a training phase, in which a series of images were presented to the participants, and a test phase, in which a series of images (including those presented in the training) were shown and it was necessary to indicate the images presented during the training [74].
At the outset of this thesis, only the data from the resting state activity and 3 choice vigilance task had been processed. As the analysis of resting state activity has already been completed [73], the focus was narrowed down to the analysis and simulation of the 3CVT task. The study of the corresponding ERP activity allows to identify some canonical components: in particular, in the occipital channels, there is the insurgence of the P1 components after 60-80 ms and of the N1 component after 110-170 ms.During this performance, the EEG activity of each patient was recorded and the resulting EEG signals coming from the occipital (PO7,PO8,O1,Oz,02) and central channels (FC1,FCz,FC2,C1,Cz,C2) were mediated in order to analyse the stimulus encoding and the decision making. The main focus of this work was the simulation of the EEG signal in the presence of the visual stimulus, in particular the reproduction of the VEP component, with the aim of reproducing the non-monotonic order observed in the results of the three conditions analysed. The latter shows a peculiar order in the EEG results of the original channels mediated for the number of patients in each condition of analysis.Thus, this result seems to require further analysis.

Chapter 5

Novel methods and results

5.1 Simulated of Visual Evoked Potentials and results

5.1.1 Analysis of VEPs dynamics

The primary outcome of this thesis was the identification of novel parameters capable of characterizing and replicating the non monotone organization of N1 peaks in EEG responses to visual stimuli lasting 200 ms within a total epoch duration of 1500 ms. Initially, to emulate an external visual stimulus, a pulse train was employed as input for nodes corresponding to the visual cortex V1. This selection was motivated by the inherent nature of the simulation, which lacks a representation of the pathway from the retina to the visual cortex. Furthermore, the decision to utilize the pulse train was based on the nature of .Regarding the network, in order to simulate the presence of a visual stimuli, weights of certain nodes needs to be modified. Specifically, weights pertaining to the visual cortex V1, the cortical region responsible for visual information processing, required modification. Given that the default weight for this region, in both left and right hemispheres, was set at 0 and was subsequently adjusted to 3.5, signifying the introduction of an external input. To model experimental conditions, where the visual stimulus was presented for a total duration of 200 ms, adjustments to the pulse train parameters were necessary. The objective was to align the variable parameters with the experimental setup. Consequently, the stimulus onset was positioned at 500 ms to accommodate plausible physiological delays and prime the network, while the duration parameter τ, representing the length of time the image was exposed to the simulated subject, and the overall duration of the experiment (T), mirroring the empirical setup, were both set at 200 and 1500 ms, respectively. Notably, aside from these parameters, alterations to the pulse train's amplitude were also feasible, theoretically ranging

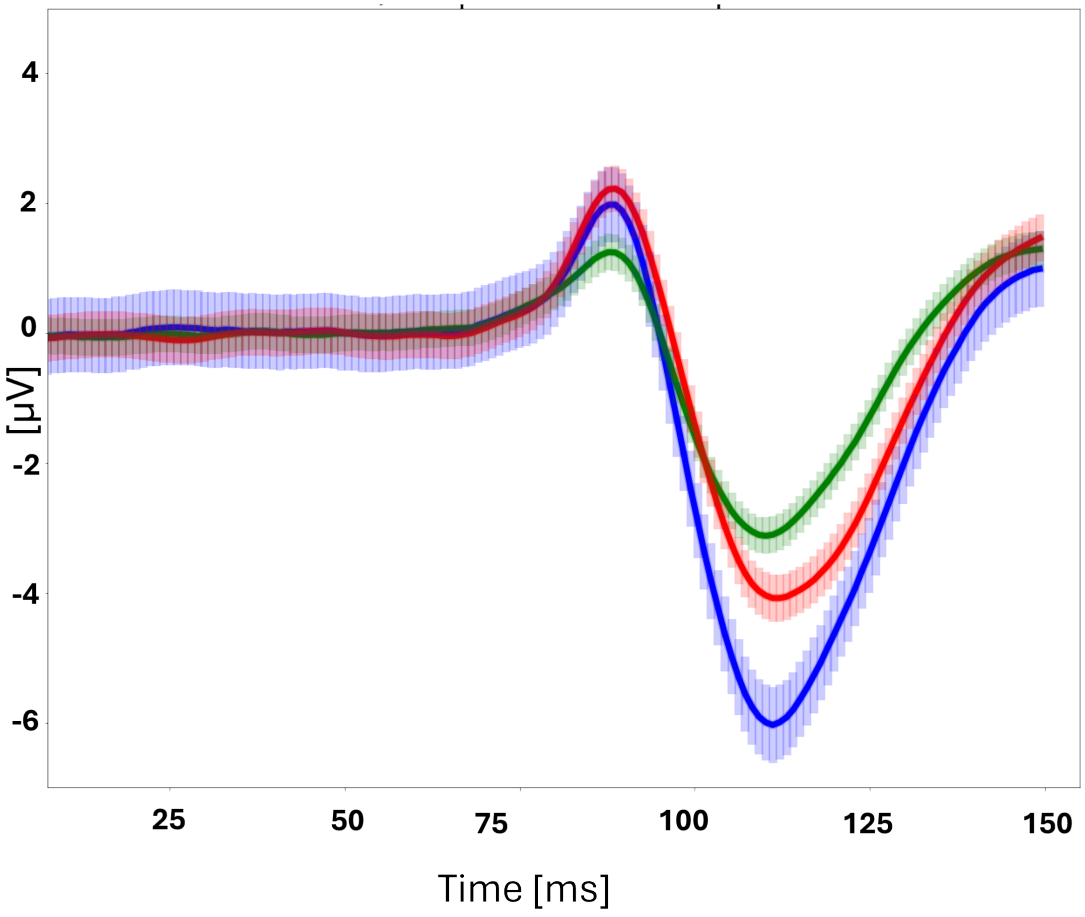

Figure 5.1: Empirical results of EEG the focus is on the VEP response

from 0 to 1, with their significance to be elucidated subsequently.
Regarding additional model parameters, modifications were made to the dynamics of both inhibitory and excitatory neuronal populations, as well as the weights of connectome tracts within the connectivity matrix as described in the work by Amato et al. (2024) [73]. Based on three distinct connectivity matrices, where in both tract length and connectivity weights were adjusted to replicate pathological scenarios of subjective cognitive decline (SCD) and mild cognitive impairment (MCI), similar adjustments were applied to the average synaptic time constants. These alterations were aimed at reproducing the changes observed in white matter fibers (reflected in the connectivity weight) and the degeneration of synaptic transmission (represented by inhibitory/excitatory reverse time constants, denoted as **a** and **b** here) [73].

Model parameter values			
Condition	Weight value	a $[s^{-1}]$	b $[s^{-1}]$
HS	0.78	0.1004	0.0476
SCD	1	0.1055	0.0370
MCI	2	0.1112	0.0257

Table 5.1: Parameters modified for each condition. Respectively: connectivity weight value,reciprocal of excitatory time constant,reciprocal of inhibitory time constant

The simulation replicates the EEG signal by computing the arithmetic mean of the outputs derived from specific channels of interest. Specifically, this calculation is performed across five channels situated over the occipital region of the scalp, corresponding to the visual cortex. These channels are denoted as O1, O2, PO4, PO5, and Oz. The decision to utilize the arithmetic mean across occipital EEG channels aligns with the experimental methodology, thereby ensuring the attainment of results that are more directly comparable and interpretable.

5.1.2 Ordering in N1 peak changing the stimulus' amplitude

As delineated earlier in this dissertation, the primary aim is to replicate the sequencing of N1 peaks and ascertain any potential correlation with the onset of dementia. To achieve this, the initial step involved evaluating whether the modifications made to the network and its dynamics (see 5.1), intended to characterize each condition, were adequate for replicating the observed empirical sequencing. Consequently, for each condition under scrutiny, an identical pulse train with consistent parameters was administered as input to distinct networks, each differing in the aforementioned introduced parameters.

However, it transpired that these modifications alone proved insufficient in reproducing the observed ERP (Event-Related Potential) behavior. Consequently, alternative solutions and additional hypotheses became imperative. Subsequent adjustments to other parameters within the utilized model were deemed unsuitable, as they pertained to contexts different to the specific description required. Instead, alterations pertaining to connectivity and time constants were explored as potential avenues for resolution.

Concerning connectivity, a systematic exploration was undertaken, varying the weight values from 0 to 2, as values exceeding 3 were deemed to represent white matter degradation beyond the scope of the analyzed cases. This exploration followed a linear progression, with fixed parameters for inhibitory/excitatory time constants. Additionally, similar analyses were conducted independently for each of the two time constant parameters, encompassing respective ranges. Subsequently, a comprehensive exploration was executed, simultaneously altering all three parameters, to evaluate the optimality of the reference parameters for the specific conditions. Despite these meticulous adjustments, alterations in the network structure alone failed to replicate the anticipated ERP ordering. Consequently, it was concluded that the network modifications, while crucial, were insufficient to achieve the desired outcome. Hence, alternative hypotheses were pursued. The proposition was posited to correlate this observed behavior with alterations in stimulus parameters.
To assess the viability of the hypothesis, a parameter exploration was conducted involving two stimulus parameters: amplitude and duration. These parameters were varied within ranges of 0.01 to 1 μV and 20 to 200 ms, respectively. Notably, this lower bound for the duration range was selected based on physiological considerations, ensuring inclusion of the time required for eye refreshment. This exploration involved simultaneous adjustments to both parameters, evaluating all possible combinations for each of the three conditions separately.

The results of the parameter exploration were visualized using three distinct heatmaps, each corresponding to a specific condition. These heatmaps illustrated how the position of the N1 minimum peak varied in response to changes in duration and amplitude. The outcomes supported the reasonableness of the hypothesis, indicating a correlation between the N1 peak position and the stimulus parameters. Notably, alterations in duration were found to have limited impact, as expected given its presumed lack of relevance to the patient condition's degradation. Conversely, amplitude emerged as a crucial factor, particularly within the range of 0.01 to 0.5 μV.
Regarding stimulus duration, the simplified nature of the simulated network—focused solely on the cortex—and the direct injection of the stimulus into the visual cortex support the assumption of a duration value slightly smaller (by at least one decimal place) than the experimental value of 200 ms.
The very same analysis was then repeated in ranges more delimited for both amplitude and duration. Moreover, a further test was conducted, displaying a binary logical value in the heatmap: true if the N1 minimum peak value was in a range of the empirical mean value $\pm$ the mean square error (mse) of the current N1 peak value and the empirical one. This was done for each condition studied, giving us possible values for the amplitude aiming in reproducing the peaks' ordering.

It was observed that to achieve this outcome, distinct values of amplitude had to be employed for each condition. Notably, these values appeared to exhibit a progressive decrease with the deterioration of the condition, transitioning from healthy subjects (HS) to mild cognitive impairment (MCI).

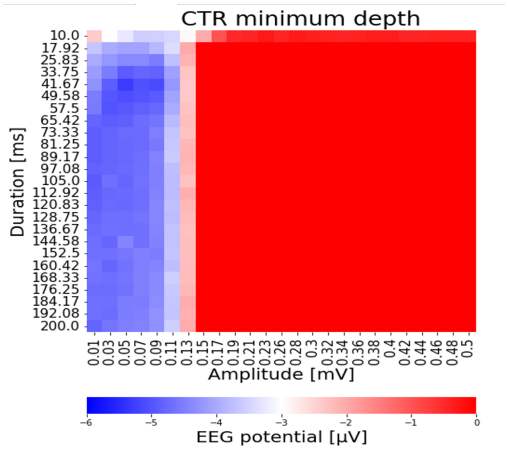

(a)

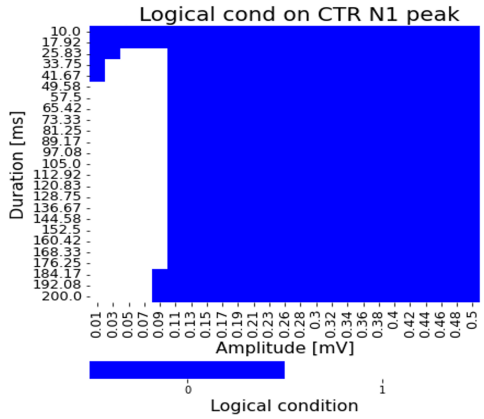

(b)

Figure 5.2: Heatmaps of parameter exploration on stimulus amplitude and duration in HC. (a) Minimum value of N1 CTR peak as a function of stimulus amplitude and duration; (b) Logical condition for the N1 HS peak ranging within the HS mean squared error.

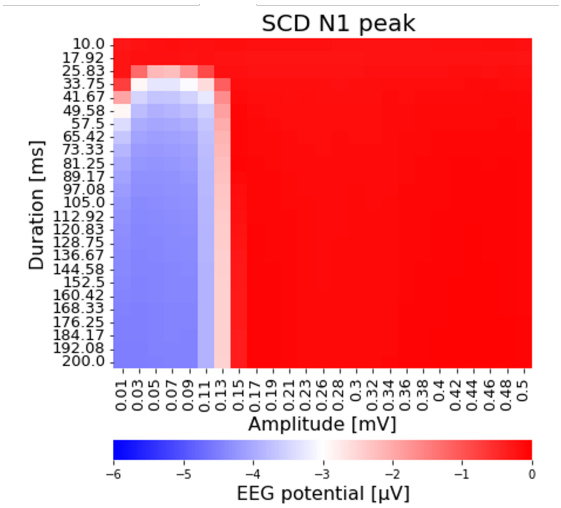

(a)

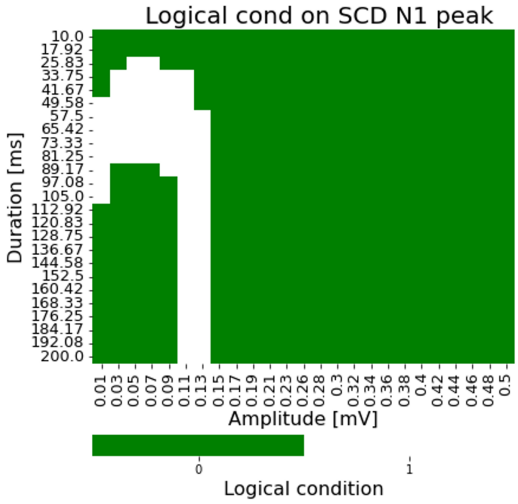

(b)

Figure 5.3: Heatmaps of parameter exploration on stimulus amplitude and duration in SCD. (a) Logical condition for the N1 SCD peak ranging within the SCD mean squared error; (b) Minimum value of N1 SCD peak as a function of stimulus amplitude and duration.

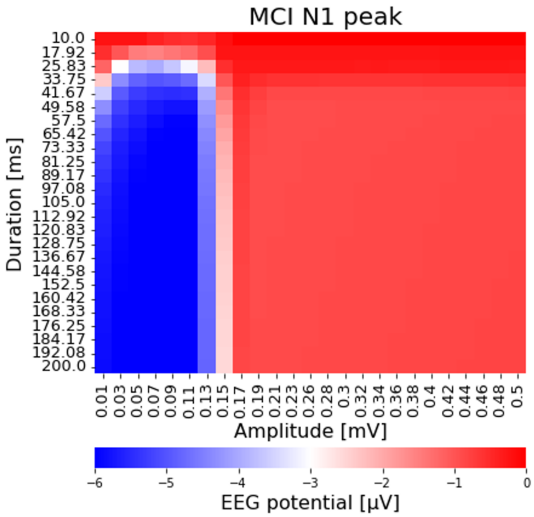

(a)

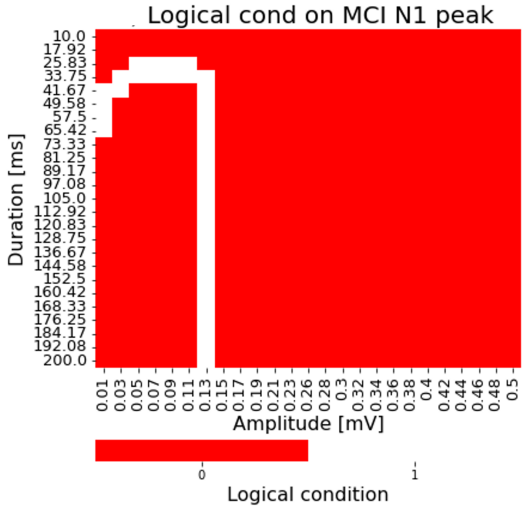

(b)

Figure 5.4: Heatmaps of parameter exploration on stimulus amplitude and duration in MCI. (a) Minimum value of N1 MCI peak as a function of stimulus amplitude and duration; (b) Logical condition for the N1 MCI peak ranging within the MCI mean squared error.

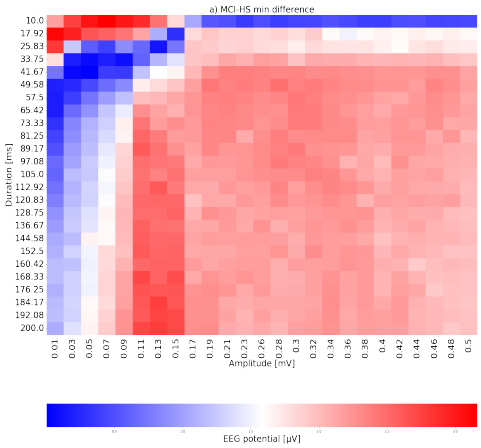

(a)

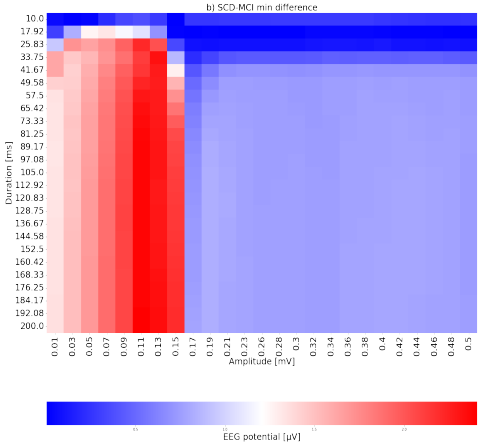

(b)

Figure 5.5: Difference matrix of N1 peak response under different conditions varying duration and amplitude (a) Difference between MCI and HS VEP peaks obtained by exploring amplitude and duration parameters (b) Difference between MCI and SCD VEP peaks obtained by exploring amplitude and duration parameters

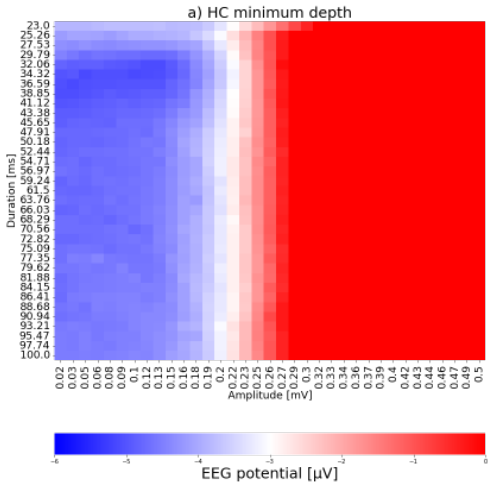

(a)

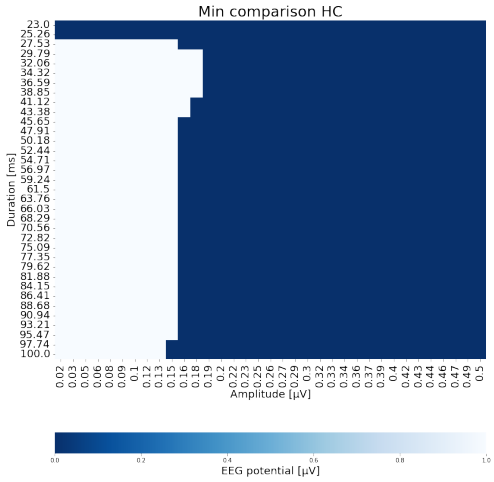

(b)

Figure 5.6: Heatmaps of parameter exploration on stimulus amplitude and duration in HS. The range considered is from 23 to 100 ms for duration and from 0.02 to 0.5 for amplitude, taking into account 35 points in each parameter. (a) Minimum value of N1 CTR peak as a function of stimulus amplitude and duration; (b) logical condition for the N1 CTR peak ranging within the CTR mean squared error;

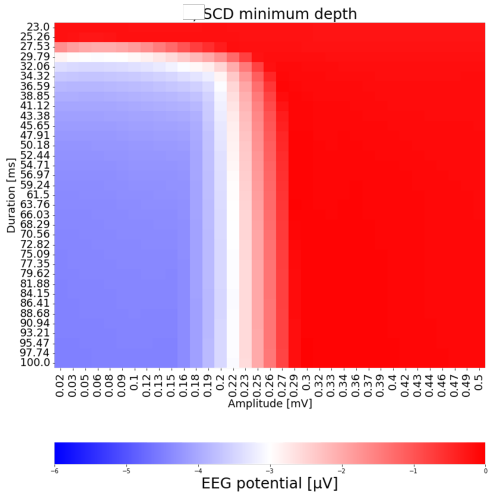

(a)

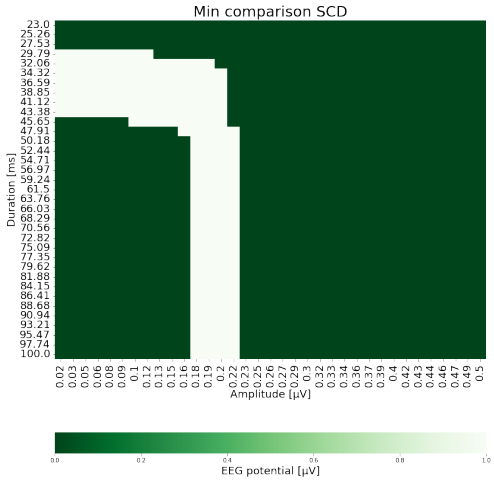

(b)

Figure 5.7: Heatmaps of parameter exploration on stimulus amplitude and duration in SCD. The range considered is from 23 to 100 ms for duration and from 0.02 to 0.5 for amplitude, taking into account 35 points in each parameter.(a) logical condition for the N1 SCD peak ranging within the SCD mean squared error; (b) Minimum value of N1 SCD peak as a function of stimulus amplitude and duration.

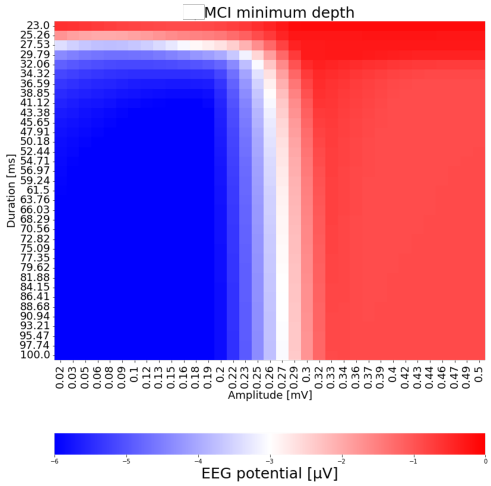

(a)

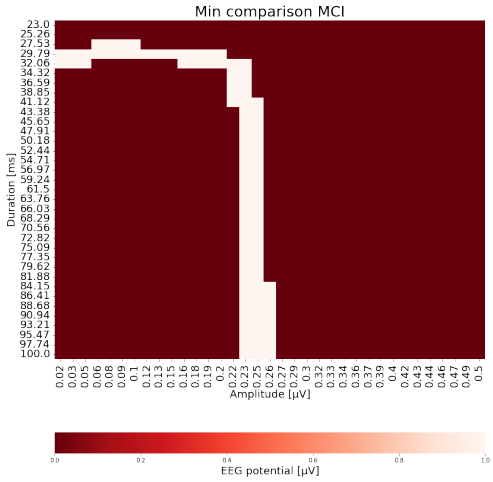

(b)

Figure 5.8: Heatmaps of parameter exploration on stimulus amplitude and duration in MCI. The range considered is from 23 to 100 ms for duration and from 0.02 to 0.5 for amplitude, taking into account 35 points in each parameter. (a) Minimum value of N1 MCI peak as a function of stimulus amplitude and duration; (b) logical condition for the N1 MCI peak ranging within the MCI mean squared error.

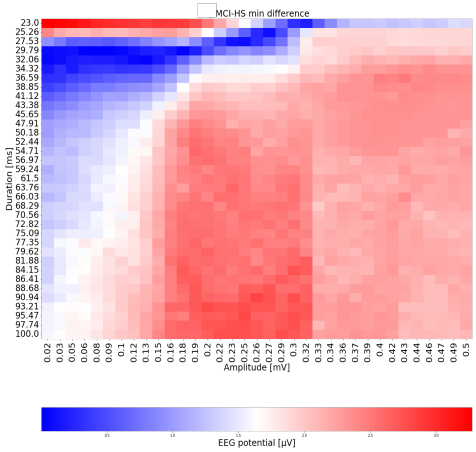

(a)

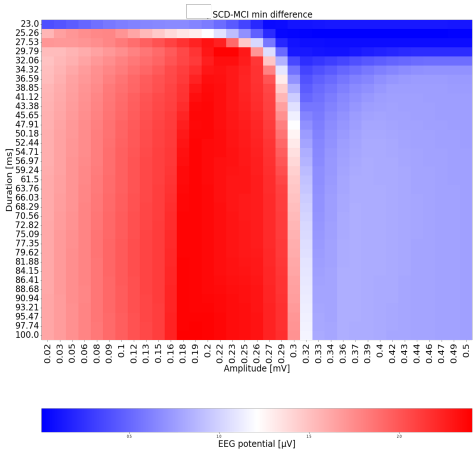

(b)

Figure 5.9: Difference matrix of N1 peak response under different conditions varying duration and amplitude (a) Difference between MCI and HS VEP peaks obtained by exploring amplitude and duration parameters (b) Difference between MCI and SCD VEP peaks obtained by exploring amplitude and duration parameters

In order to find the optimal amplitude parameters, an optimization algorithm was implemented. The main idea was to iteratively update the value of the amplitude until convergence, which corresponds to a value of the N1 peak that is the 95% of the experimental one. For each iteration, the minimum corresponding to the current amplitude value is taken, then the new amplitude is found as the difference between the previous amplitude value and the Mean Absolute Error (MAE) between the N1 peak value found in the previous step and the N1 peak experimental value, multiplied by a chosen learning rate.

$$MAE = \frac{\sum_{i=0}^{n} |y_i - x_i|}{n} \tag{5.1}$$

Where x_i is the empirical value, y_i the observed value and n is the number of samples considered (here only one).

Algorithm 1 Pseudo code of the fitting algorithm

$i \leftarrow 1$
$NumIterations \leftarrow nIter$
$\alpha \leftarrow \alpha_{lr}$ ▷ learning rate
$amp \leftarrow InitialAmplitude$ ▷ amplitude
$MinValue \leftarrow -\infty$ ▷ starting min value

for $i \in NumIterations$ **do**

$MinValue \leftarrow simulation(channels, amp, \tau)$
$amp_{new} = amp - \alpha|MinValue - MinEmpirical|$

if $MinValue \leq 0.90(MinEmpirical)$ **then**
break
end if

$amp = amp_{new}$

end for

Surprisingly, the best-approximating amplitude values were different for each condition, encouraging further investigations.
In order to have a counter-evidence to the hypothesis made, and not only to refer to the minimum of the VEP, the same analysis was repeated taking into account the integral of the N1 curve. The integral was calculated according to

the *Simpson-Cavalieri* rule, a numerical integration method that approximates the definite integral of a function with a quadratic polynomial on each interval of the partition.
Parameter exploration was done for both amplitude and duration, using the same ranges as those used to explore the N1 peaks and computing the integral for each combination. In order to find the optimal amplitude values for each condition, and to see if they correspond to those found with the analysis of the negative peaks, the fitting algorithm used previously was adapted to the integral analysis.

Algorithm 2 Pseudo code of the fitting algorithm for the integral

$i \leftarrow 1$
$NumIterations \leftarrow nIter$
$\alpha \leftarrow \alpha_{lr}$ ▷ learning rate
$amp \leftarrow InitialAmplitude$ ▷ amplitude
$IntValue \leftarrow -\infty$ ▷ starting integral value

for $i \in NumIterations$ **do**

$IntValue \leftarrow simulation(channels, amp, \tau)$
$amp_{new} = amp - \alpha|IntValue - IntEmpirical|$

if $|IntValue| \geq 0.85|IntEmpirical|$ **then**
break
end if

$amp = amp_{new}$

end for

The results obtained from this analysis were similar to those obtained from the N1 minimum, suggesting the robustness of the hypothesis.

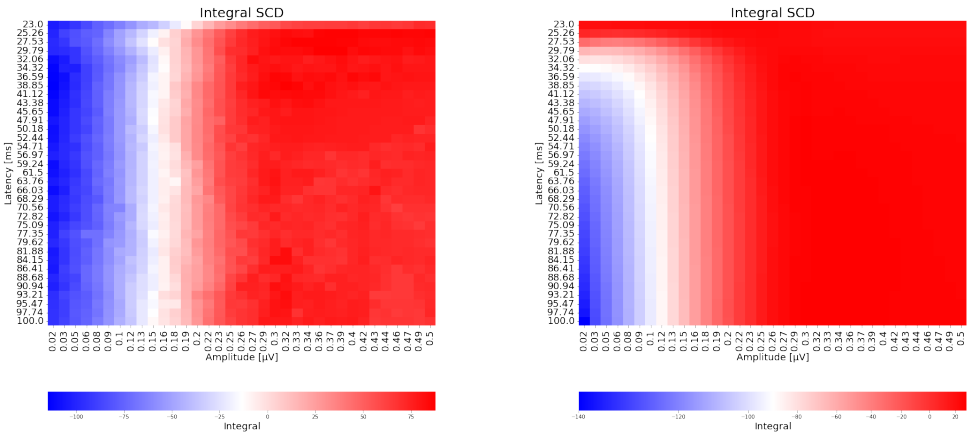

(a) **(b)**

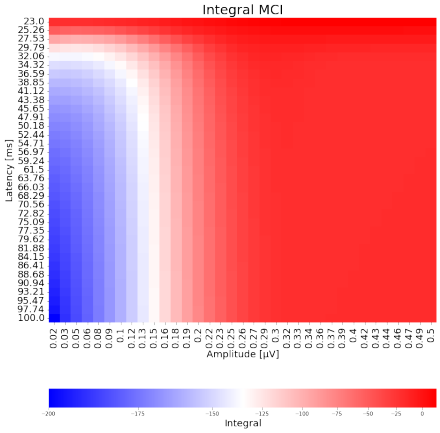

(c)

Figure 5.10: Heatmaps of parameter exploration on stimulus amplitude and duration in different conditions The range considered is from 23 to 100 ms for duration and from 0.02 to 0.5 for amplitude, taking into account 35 points in each parameter.(a) Integral value of N1 HS as a function of stimulus amplitude and duration. (b) Integral value of N1 SCD as a function of stimulus amplitude and duration. (b) Integral value of N1 MCI as a function of stimulus amplitude and duration.

The newly obtained amplitude parameters, derived from fitting, were integrated into the corresponding functions to simulate the EEG outcomes. The objective was to replicate a trend similar to the empirical data, particularly focusing on the ordering of the Visual Evoked Potential (VEP) curve. To mimic the experimental setup, the noise seed value of the model was increased, resulting in EEG outcomes that fluctuated akin to those of a single individual. For each condition, a simulation was executed a number of times equivalent to the number of individuals in the experimental group. This process generated three sets of VEP outcome results, which were subsequently averaged across simulations for each condition, yielding three averaged EEG signals.These averaged EEG signals were then juxtaposed with the empirical results. The randomization applied to each simulation helped attenuate fluctuations around zero prior to the stimulus onset. Furthermore, the mean square error was computed for each category, demonstrating the distinctiveness of each curve.
In summary, this methodology allowed for the generation of simulated EEG signals that closely mirrored empirical data, facilitating comparison and analysis.

Condition	Amplitude values
HS	0.22750
SCD	0.06336
MCI	0.05368

Table 5.2: Optimal amplitude value for each condition given by fitting algorithm.

The chosen parameters for the amplitude, displayed in the table 5.2, are then inserted in the respective condition-specific function, and the result obtained is displayed in 5.11. Indeed, by progressively reducing the stimulus amplitude, and thus physiologically diminishing its intensity, it becomes feasible to replicate the non-monotonic ordering observed. Specifically, this results in the lower peak occurring in healthy subjects, the middle peak in MCI condition, and the smallest peak in subjective cognitive decline. This observation suggests a correlation between the intensity of the stimulus and the ordering of peaks in the EEG signal, providing valuable insights into the relationship between stimulus strength and cognitive responses across different stages of cognitive impairment. Notice that the descent of the EEG signal,corresponding to the onset of VEP, starts after approximately 50 ms from the stimulus' advent, as it happens in the experiment, and the peak is reached after about 125-130 ms, about 20 ms in advice with respect to the real

case.

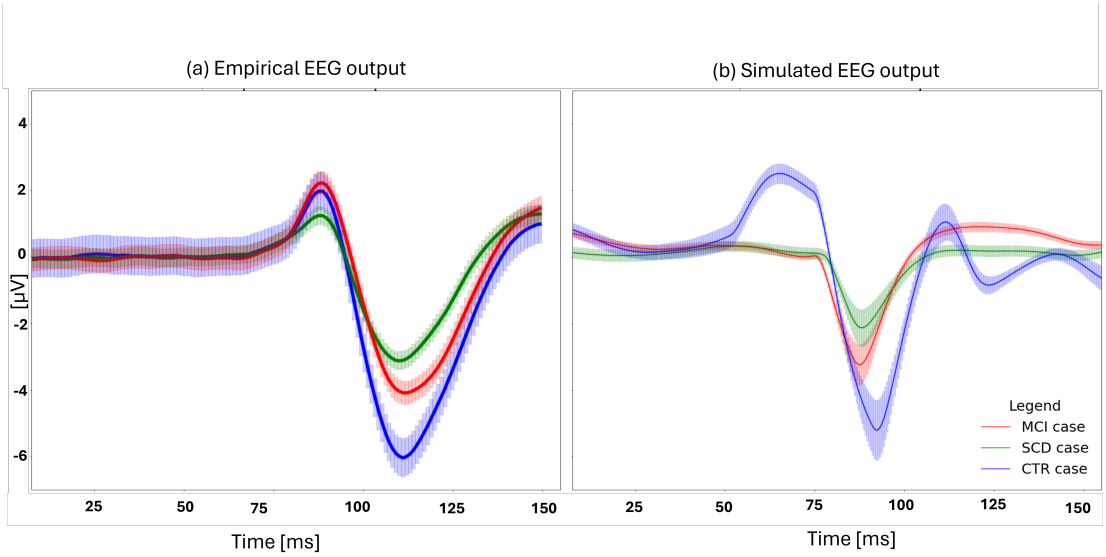

Figure 5.11: Comparison between simulated and empirical VEPs. Empirical EEG signals coming from each condition seems to have a peculiar ordering, thus they required further analysis. In particular, MCI and HS N1 component seems to be more close with respect to MCI and SCD or HS and SCD.Moreover, a particular ordering is showing, having the outcome ordering non monotone in comparison with the worsening of the condition as one can expecting, since SCD subjects presents on average outcomes that are worse with respect to the other conditions.The result is obtained by changing the values of the stimulus amplitude in the hypothesis of considering also the effect of visual path degeneration by means of this parameter. The values were found to best fit the mean values of the experiment by parameter exploration and are different according to the condition treated, the duration parameter is constant and equal in all three cases (50 ms in the simulation, 200 ms in the experiment). a) Empirical results, the shading is the mean squared error (MSE) on subjects considered; b) Simulation results, the shading is obtained as the mean square error for each simulation.

The observed reduction in amplitude from healthy subjects to mild cognitive impairment suggests a potential deterioration in the optical pathway from the eye to the visual cortex. This situation can be conceptualized by modeling an attenuated signal as input to the visual cortex V1. The implications and underlying causes of these findings will be further explored and discussed subsequently.
To gain deeper insight into these results, it may be beneficial to investigate the dementia continuum by exploring intermediate conditions within the spectrum of cognitive impairment considered. This approach will help determine the stability

of the observed trend and provide additional understanding of the progression of cognitive decline in relation to visual processing.

5.2 Analysis of the dementia continuum

As illustrated in Figure 5.1 of the concluding paragraph and in the subsequent discussion, the alterations in peak values were discovered to exhibit a non-monotonic trend with respect to the parameters, notably manifesting a change in amplitude. This adjustment facilitated the replication of the observed ordering evident in analytical results. Additionally, it is noteworthy that a progressive reduction in amplitude was observed from controls to individuals with mild cognitive impairment. These findings underscore the significance of stimulus amplitude in shaping the observed EEG responses, and the finding of a reasonable biological interpetation could highlight a potential biomarker for cognitive decline across varying stages of impairment.

Model parameter values				
Condition	Weight value	excitatory neurons dynamics	inhibitory neurons dynamics	Amplitude values
HS	0.78	0.1004	0.0476	0.1250
SCD	1	0.1055	0.0370	0.0780
MCI	2	0.1112	0.0257	00557

Table 5.3: Values of parameters in connectivity weight,excitatory/inhibitory dynamics and stimulus' amplitude for each analyzed condition. The parameters are found by fitting the model to the experimental case.

Indeed, exploring intermediate stages between the healthy condition and subjective cognitive decline , progressing towards mild cognitive impairment, presents a promising avenue for further investigation. From the examination of these intermediate stages, it could be possible gain deeper insights into the gradual progression of cognitive decline and its associated neural markers. This approach allows for a more nuanced understanding of the continuum of cognitive impairment, highlighting subtle changes in brain function and structure that occur along the trajectory from normal aging to pathological conditions. Moreover, a focus on the intermediate stages can help to gain insight on transitional phases, where the cognitive decline

has started but has not yet reached a pathological condition to diagnose MCI. The objective was to prove that changes both in the network and in the input are capable to show a progressive impairment of cognitive function, following the same non-monotone trend observed in the three main cases alone. Computationally ,this was done considering changing the inhibitory and excitatory neurons dynamics and of the weights of connectivity, also with a linear interpolation of the amplitude values.
Computationally, the investigation was done altering linearly the dynamics of inhibitory and excitatory neurons, as well as the weights of connectivity, across intermediate stages between healthy aging and mild cognitive impairment. Additionally, a linear interpolation approach was employed to modulate the amplitude values, allowing for a gradual transition between the healthy state and cognitive decline.
Adjusting the connectivity weights and the neuronal population dynamics as well as smoothly varying the stimulus amplitude, the computational model simulated the changes in the network occurring along the cognitive decline.
In the computational analysis, a total of 25 points were considered within the spectrum between the extremes of each tract, transitioning from healthy aging to subjective cognitive decline and from SCD to mild cognitive impairment . At each of these 25 points, the dynamical parameters of excitatory and inhibitory neurons, the weights of the connectivity matrix, and the amplitude were adjusted linearly according to the respective extremes of the tract.
For the transition from healthy aging to SCD, the dynamics of excitatory and inhibitory neurons were altered from 0.1004 to 0.1055 and from 0.0476 to 0.0370, respectively. The weight of the connectivity matrix changed from 0.78 to 1, and the amplitude varied from 0.455 to 0.0780. Similarly, for the transition from SCD to MCI, the same parameters were linearly adjusted across 25 intermediate points. The dynamics of inhibitory neurons changed from 0.0370 to 0.0257, while those of excitatory neurons transitioned from 0.1005 to 0.112. The weight of the connectivity matrix evolved from 1 to 2, and the amplitude decreased from 0.077 to 0.0557.
The results of this continuum analysis are depicted in Figure 5.12, providing insights into the progressive changes in neural dynamics and connectivity across the spectrum from healthy aging to mild cognitive impairment.

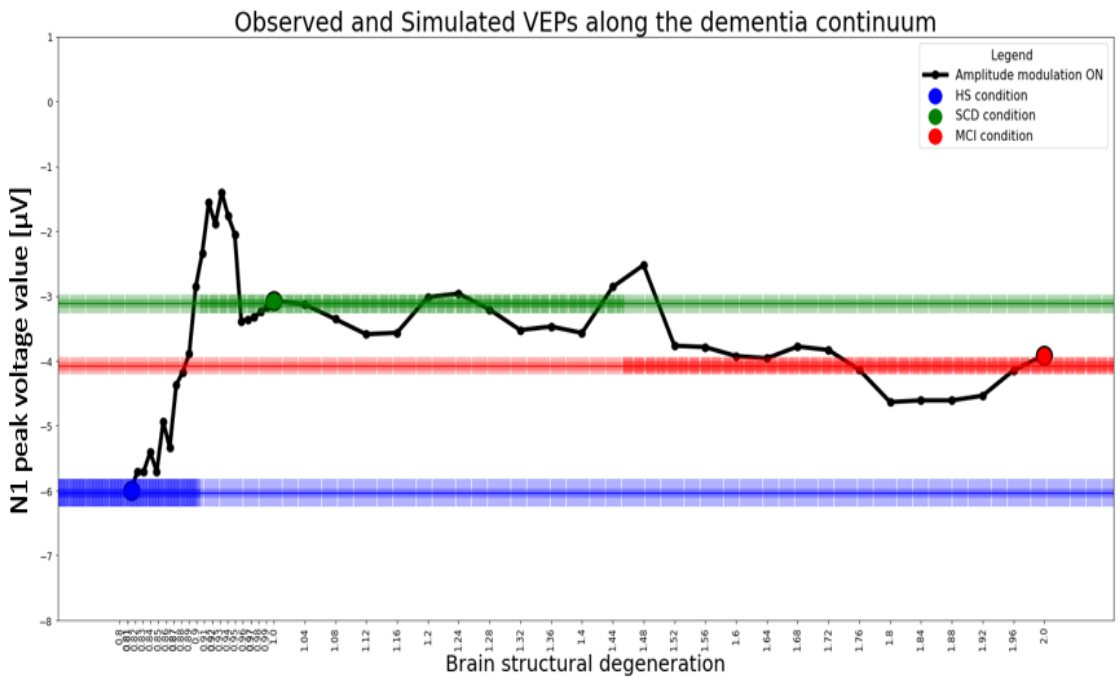

Figure 5.12: Effect of the stimulus' amplitude modulation along the dementia continuum, plotting the N1 peak.
The thick black line represents a study in the continuum of the three conditions,from Healthy subjects (HS) to MCI. The result is obtained changing linearly the parameters associated to the dynamics of inhibitory and excitatory populations,the one of the connectivity weight and the stimulus' amplitude.25 intermediate point were considered between each next condition studied. Starting from HS, we have an abrupt growing in the voltage value of the N1 peak,followed by a jump to values in SCD range,right before entering in the specific condition; concerning SCD to MCI range,for the first half the trend is mostly constant around the SCD experimental value, then a small growth followed by a jump is again present right before entering a sort of pre-MCI condition. The big colored dots are referring to the value of the N1 peak for each condition, obtained with a change in the amplitude .The horizontal shading with blu/green/red colors is referred to empirical N1 peak values (mean and MSE) for HS/SCD/MCI subjects. The referring parameters for those points are the ones in Table 5.3

The observed trend in the obtained curve is notable. From HS to SCD there is a rapid growth in the N1 peak value, suggesting a transitional state from one condition to the other.This is followed by an abrupt drop to lower values just before entering the SCD condition, suggesting a transitional phase marked by neural changes indicative of impending cognitive decline. Following this transition, the

curve exhibits an oscillatory behavior around the mean empirical value of the SCD N1 peak. This oscillation may reflect fluctuations in neural activity or compensatory mechanisms as the brain attempts to adapt to the emerging cognitive challenges associated with SCD.Subsequently, there is another smaller jump observed in a pre-MCI state, indicating further decline in neural function or cognitive abilities. This is followed by continued oscillation around the mean value of the empirical MCI peak, reflecting ongoing fluctuations in neural activity and cognitive function characteristic of the MCI stage.

This observed pattern suggests a complex interplay of neural changes occurring across the continuum from healthy aging to cognitive decline. The transitions between cognitive states are marked by distinct changes in neural dynamics, with periods of rapid growth, abrupt drops, and oscillatory behavior, reflecting the multifaceted nature of cognitive decline.

To further elucidate the credibility of the amplitude reduction hypothesis and to validate the results obtained in the continuum experiment,the same analysis was replicated under a "zero hypothesis" condition. In this environment, the network parameters were modified linearly as before, but the amplitude values were held constant at a fixed value for all the simulations from HS to MCI. The simulations was repeated for ten different amplitude values, from 0.03 to 1, and the results are shown in figure 5.13. For amplitude values smaller than 0.05,the curves generated from the continuum analysis are consistently positioned above those with amplitude modulation. Moreover, as the amplitude value decreases, the "zero-hypothesis" curves occupy progressively higher positions relative to the curves with amplitude modulation.The very same happens for values higher than 0.05, but in an opposite manner : the curves occupying progressively lower positions with respect to the main modulated curve as the amplitude value increase . Moreover, for values greater than 0.7, the curves tends to overlap.From this analysis, it can be inferred that amplitude is to work as a form of modulation of the curve's offset, effectively positioning it within the appropriate range corresponding to the observed condition.To further demonstrate the correspondence between the simulated results and the observed conditions, horizontal lines were overlaid on the graph representing the empirical values of the N1 peak. Additionally, shading was applied to each line, corresponding to a set shading of acceptable values around the empirical results , providing a visual representation of the accuracy of the simulated results relative to the empirical data.

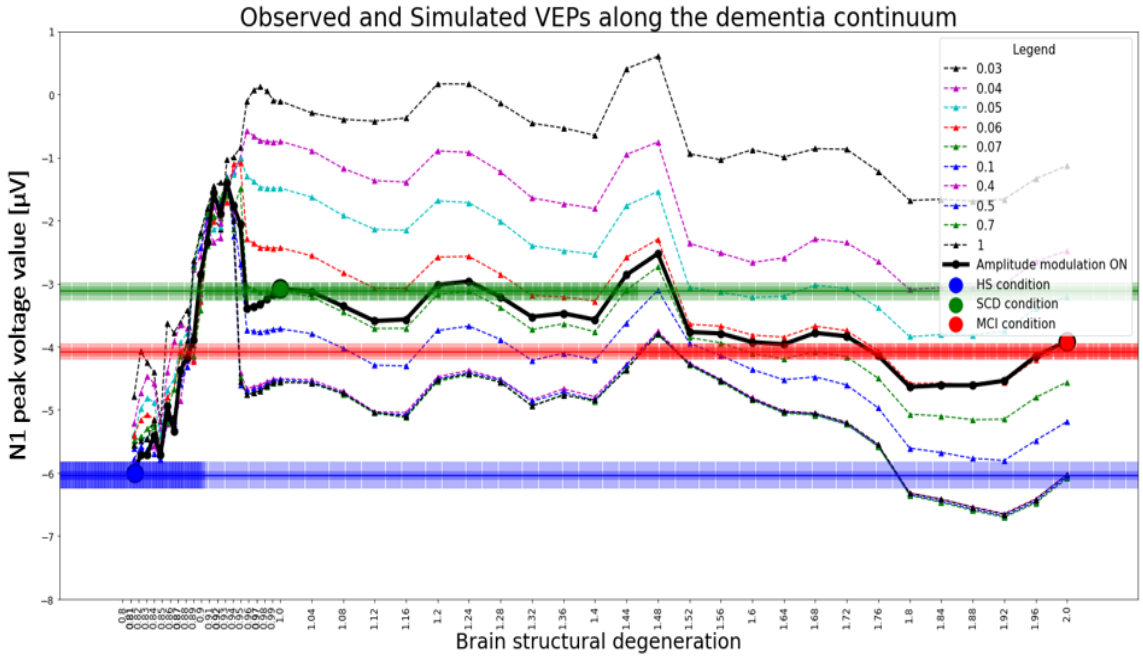

Figure 5.13: Effect of the stimulus' amplitude modulation along the dementia continuum, plotting the N1 peak. Zero-hypotesis comparison. The thick black line represents a study in the continuum of the three conditions, changing linearly the parameters associated to the dynamics and to the connectome but also the stimulus' amplitude (see Fig 5.12). The dashed lines are representing the same study, changing the inhibitory/excitatory dynamics and the connectivity weight linearly but keeping the amplitude value constant to a specific value. Moreover,for amplitude values smaller than 0.07, the corresponding curves are upper placed with respect to the black line,taking higher positions lowering the parameter and, for greater amplitude values, the exact opposite is happening notice that, when the amplitude is greater than 0.5, the different curves coincides.Note that the amplitude changes seem to work as an offset for the curve, placing it in the right range for the condition considered.

One last analysis was to see more closely what happens in the range of brain structural degeneration around the first jump from HS to a pre-SCD condition. First, a more accurate and range-specific interpolation was done, considering 25 points between the two extremes considered (so 0.9000 and 1) and changing again linearly the network and dynamical parameters as well as the stimulus' amplitude. As shown in figure 5.5,the very same behaviour is observed, and a jump is still present around 0.925. Subsequently, a more closed look was done around the jump,again in a range from 0.9250 to 0.9365.

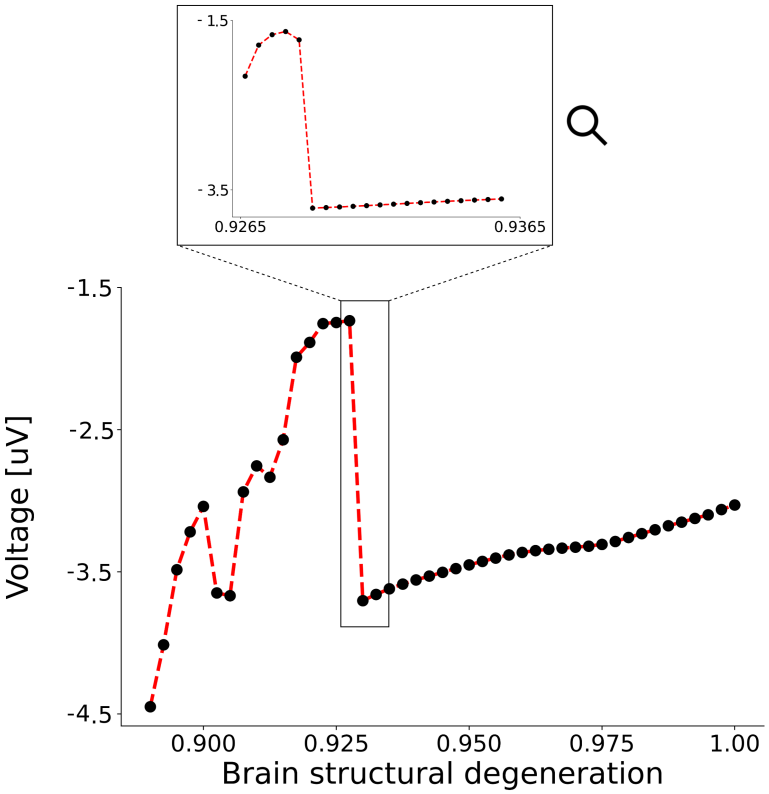

Figure 5.14: More detailed study of the HS-SCD jump transition. To better understand what happens in the abrupt jump right before entering the SCD condition, values of degeneration in a range from 0.9 to 1 were considered, taking 50 values of amplitude,dynamics and connectivity between the two extremes, to see if the jump was still there. The plot shows the result of this more detailed interpolation, displaying the very same trend.Thus a further analysis was done, considering 20 points of linear evolution of the very same parameters, but in a closer range around the jump (from 0.9250 to 0.9365), showing the permanence of the abrupt transition.

Results of those continuum analysis shows, from a value of -6μV, first a growth in the voltage value associated to the N1 peak, thus values more close to 0, then an abrupt jump to lower values in a range -3μV, and finally descend to an intermediate values range around -4μV.

The implementation of this more detailed investigation and the subsequent results showed the presence of an abrupt transition from one condition to the subsequent, more impaired,one. This transition is particularly pronounced in the shift from healthy aging individuals to those with SCD. Nevertheless, this behavior

can be interpreted as a potential marker indicating the transition from one condition to the next.
With further analysis and validation, it may be possible to evaluate the stage of disease progression in an individual and assess the likelihood of developing Alzheimer's disease or other forms of dementia. By identifying distinct neural signatures associated with different stages of cognitive decline, clinicians may be better equipped to diagnose and prognosticate the progression of neurodegenerative diseases. Additionally, this knowledge could inform the development of targeted interventions aimed at delaying or preventing the onset of dementia in at-risk individuals.
Those results suggest the crucial role of the stimulus amplitude parameter in this analysis.The latter can be interpreted in physiological manner as the intensity of the external visual stimulus.The progressive attenuation in the amplitude can be interpreted as the degradation of the path from retina to visual cortex .

Chapter 6

Conclusion

6.1 Discussion and future developments

From the analysis and hypothesis presented, it seems plausible to hypothesise that the non-monotonic ordering of the first negative peak of the VEP in the EEG signal under the conditions considered may be due to a progressive degradation of the retina-thalamus-cortex pathway where the visual signal is processed. In the simulation discussed here, this degradation is modelled as a decreasing amplitude of the visual stimulus given as input to the visual cortex nodes V1. This choice can also be justified by the fact that the simulation given by The Virtual Brain is only of the cerebral cortex, without models of the thalamus and the retina, which are essential in the stimulus process. In summary, the reduction in stimulus amplitude represents a reduction in the brain's ability to process the visual stimulus.
In dementia, and particularly in Alzheimer's disease, many patients present with visuospatial impairment, retinal thinning and optic nerve damage. Moreover, structural changes in the retina are already present in mild cognitive impairment [75]. In particular, studies confirm that the reduction of retinal ganglion cells (RGS) and axons can also affect the visual pathway, reducing the density of optic nerve fibres and impairing the visual process [76, 77].In particular, axon loss appears to affect the magnocellular cells of the lateral geniculate nucleus, which are involved in light contrast detection [77]. Additional VEP and electroretinogram (ERG) studies confirm that neural transmission from the retina to the primary visual cortex is impaired in AD, with a significant delay in neural transmission and reduced amplitude of the N200 peak of the motion-onset VEP [78].
Therefore, it is reasonable to assume that differential stimulus processing could be due to a delay in neural transmission in the retina-cortex pathway [76] or to a visual attentional impairment due to disease progression [78]. These findings pave the way to suggest causal mechanisms for N100 VEP dynamics, which could be

explored by in vivo investigation of retina-V1 pathway integrity in both animal models and humans.
The correlation between brain degeneration and the position of the N1 peak could potentially be interpreted as an expression of one of the numerous pathways through which the disease may manifest itself. It is obvious that the trend followed by the curve allows for further analysis and assumptions to be made on the result obtained. For example, one possible development is mapping the relationship between the minimum position and the age of the patients involved, to discern if there is a correlation with ageing and whether it is more likely to develop the first clinical symptoms of the disease and how to prevent its onset. It is therefore reasonable to assume that the analysis of EEG signals can be a useful tool for understanding the development and progression of dementia, becoming an economical and non-invasive tool to assist in the diagnosis of the disease or as a supporting method to other diagnostic techniques. With further analysis and validation, it may be possible to assess the stage of disease progression in an individual and the likelihood of developing Alzheimer's disease or other forms of dementia. By identifying distinct neural signatures associated with different stages of cognitive decline, clinicians may be better equipped to diagnose and predict the progression of neurodegenerative diseases. In addition, this knowledge could inform the development of targeted interventions aimed at delaying or preventing the onset of dementia in at-risk individuals.
In this picture, The Virtual Brain appears to be a valid tool for validating experimental results and could also be useful for implementing further investigations on given experiments. Furthermore, the open source nature of this software allows for modifying existing models and supports the creation of new ones from scratch.
Future developments may include the generation of new and more complete computational models capable of simulating other parts of the brain (e.g. the thalamus) in order to gain insight into the development of dementia and its onset, and to be able to differentiate between the multiple forms of this plethora of diseases. Furthermore, a deeper understanding of the disease with the aid of computational tools could prove helpful for early diagnosis, enabling the detection of the disease prior to the manifestation of overt symptoms. Therefore, experimental analysis using computational models appears to lead the way for novel research approaches into the causes and progression of these diseases, aiding in the discovery of new biomarkers and, hopefully, contributing to the formulation of new treatments.

Appendix A

Appendix

Link to the code repository : `https://github.com/MichelaRocchetti/modeling_degeneration_VEP`

Bibliography

[1] Richard Mayeux. «Alzheimer's disease: epidemiology». In: *Handbook of clinical neurology* 89 (2008), pp. 195–205 (cit. on p. 1).

[2] Alberto Serrano-Pozo, Matthew P Frosch, Eliezer Masliah, and Bradley T Hyman. «Neuropathological alterations in Alzheimer disease». In: *Cold Spring Harbor perspectives in medicine* 1.1 (2011), a006189 (cit. on pp. 1, 9).

[3] Leon Stefanovski et al. «Bridging scales in alzheimer's disease: Biological framework for brain simulation with the virtual brain». In: *Frontiers in Neuroinformatics* 15 (2021), p. 630172 (cit. on p. 1).

[4] Roxana A Stefanescu and Viktor K Jirsa. «A low dimensional description of globally coupled heterogeneous neural networks of excitatory and inhibitory neurons». In: *PLoS computational biology* 4.11 (2008), e1000219 (cit. on pp. 1, 17).

[5] Argonde C van Harten, Michelle M Mielke, Dana M Swenson-Dravis, Clinton E Hagen, Kelly K Edwards, Rosebud O Roberts, Yonas E Geda, David S Knopman, and Ronald C Petersen. «Subjective cognitive decline and risk of MCI: The Mayo Clinic Study of Aging». In: *Neurology* 91.4 (2018), e300–e312 (cit. on p. 1).

[6] Ronald C Petersen et al. «Current concepts in mild cognitive impairment». In: *Archives of neurology* 58.12 (2001), pp. 1985–1992 (cit. on p. 2).

[7] Paula Sanz Leon, Stuart A Knock, M Marmaduke Woodman, Lia Domide, Jochen Mersmann, Anthony R McIntosh, and Viktor Jirsa. «The Virtual Brain: a simulator of primate brain network dynamics». In: *Frontiers in neuroinformatics* 7 (2013), p. 10 (cit. on pp. 2, 26).

[8] Paula Sanz-Leon, Stuart A Knock, Andreas Spiegler, and Viktor K Jirsa. «Mathematical framework for large-scale brain network modeling in The Virtual Brain». In: *Neuroimage* 111 (2015), pp. 385–430 (cit. on pp. 2, 3, 18, 20, 26, 27).

[9] John L Robinson et al. «Neurodegenerative disease concomitant proteinopathies are prevalent, age-related and APOE4-associated». In: *Brain* 141.7 (2018), pp. 2181–2193 (cit. on p. 2).

[10] Jeffrey L Cummings and Greg Cole. «Alzheimer disease». In: *Jama* 287.18 (2002), pp. 2335–2338 (cit. on p. 4).

[11] Christiane Reitz, Carol Brayne, and Richard Mayeux. «Epidemiology of Alzheimer disease». In: *Nature Reviews Neurology* 7.3 (2011), pp. 137–152 (cit. on p. 4).

[12] Rupert McShane, Almudena Areosa Sastre, and Neda Minakaran. «Memantine for dementia». In: *Cochrane database of systematic reviews* 2 (2006) (cit. on p. 4).

[13] Barry Reisberg, Rachelle Doody, Albrecht Stöffler, Frederick Schmitt, Steven Ferris, and Hans Jörg Möbius. «Memantine in moderate-to-severe Alzheimer's disease». In: *New England Journal of Medicine* 348.14 (2003), pp. 1333–1341 (cit. on p. 4).

[14] Vincenzo Nicola Talesa. «Acetylcholinesterase in Alzheimer's disease». In: *Mechanisms of ageing and development* 122.16 (2001), pp. 1961–1969 (cit. on p. 4).

[15] Michael E Hasselmo. «The role of acetylcholine in learning and memory». In: *Current opinion in neurobiology* 16.6 (2006), pp. 710–715 (cit. on p. 4).

[16] Dennis J Selkoe. «Alzheimer's disease results from the cerebral accumulation and cytotoxicity of amyloid\beta-protein». In: *Journal of Alzheimer's disease* 3.1 (2001), pp. 75–82 (cit. on p. 5).

[17] John E Morley and Susan A Farr. «The role of amyloid-beta in the regulation of memory». In: *Biochemical pharmacology* 88.4 (2014), pp. 479–485 (cit. on p. 5).

[18] Michael A Castello and Salvador Soriano. «On the origin of Alzheimer's disease. Trials and tribulations of the amyloid hypothesis». In: *Ageing research reviews* 13 (2014), pp. 10–12 (cit. on p. 5).

[19] Si-Qiang Ren, Wen Yao, Jing-Zhi Yan, Chunhui Jin, Jia-Jun Yin, Jianmin Yuan, Shui Yu, and Zaohuo Cheng. «Amyloid β causes excitation/inhibition imbalance through dopamine receptor 1-dependent disruption of fast-spiking GABAergic input in anterior cingulate cortex». In: *Scientific reports* 8.1 (2018), p. 302 (cit. on p. 5).

[20] Gunnar K Gouras, Claudia G Almeida, and Reisuke H Takahashi. «Intraneuronal Aβ accumulation and origin of plaques in Alzheimer's disease». In: *Neurobiology of aging* 26.9 (2005), pp. 1235–1244 (cit. on p. 5).

[21] Fernando Maestú, Willem de Haan, Marc Aurel Busche, and Javier DeFelipe. «Neuronal excitation/inhibition imbalance: core element of a translational perspective on Alzheimer pathophysiology». In: *Ageing Research Reviews* 69 (2021), p. 101372 (cit. on p. 5).

[22] Willem De Haan, Katherine Mott, Elisabeth CW Van Straaten, Philip Scheltens, and Cornelis J Stam. «Activity dependent degeneration explains hub vulnerability in Alzheimer's disease». In: (2012) (cit. on p. 5).

[23] Willem de Haan, Elisabeth CW van Straaten, Alida A Gouw, and Cornelis J Stam. «Altering neuronal excitability to preserve network connectivity in a computational model of Alzheimer's disease». In: *PLoS computational biology* 13.9 (2017), e1005707 (cit. on p. 5).

[24] Madeleine R Brown, Sheena E Radford, and Eric W Hewitt. «Modulation of β-amyloid fibril formation in Alzheimer's disease by microglia and infection». In: *Frontiers in molecular neuroscience* 13 (2020), p. 609073 (cit. on p. 5).

[25] Patrick L McGeer, EG McGeer, and K Yasojima. *Alzheimer disease and neuroinflammation*. Springer, 2000 (cit. on p. 5).

[26] Agneta Nordberg. «PET imaging of amyloid in Alzheimer's disease». In: *The lancet neurology* 3.9 (2004), pp. 519–527 (cit. on p. 6).

[27] Khalid Iqbal, Fei Liu, C-X Gong, and Inge Grundke-Iqbal. «Tau in Alzheimer disease and related tauopathies». In: *Current Alzheimer Research* 7.8 (2010), pp. 656–664 (cit. on pp. 5, 6).

[28] Tong Guo, Wendy Noble, and Diane P Hanger. «Roles of tau protein in health and disease». In: *Acta neuropathologica* 133 (2017), pp. 665–704 (cit. on p. 6).

[29] Michala Kolarova, Francisco Garcıa-Sierra, Ales Bartos, Jan Ricny, Daniela Ripova, et al. «Structure and pathology of tau protein in Alzheimer disease». In: *International journal of Alzheimer's disease* 2012 (2012) (cit. on p. 6).

[30] Serge Gauthier et al. «Mild cognitive impairment». In: *The lancet* 367.9518 (2006), pp. 1262–1270 (cit. on p. 7).

[31] Heiko Braak and Eva Braak. «Neuropathological stageing of Alzheimer-related changes». In: *Acta neuropathologica* 82.4 (1991), pp. 239–259 (cit. on p. 7).

[32] Frank Jessen et al. «A conceptual framework for research on subjective cognitive decline in preclinical Alzheimer's disease». In: *Alzheimer's & dementia* 10.6 (2014), pp. 844–852 (cit. on p. 9).

[33] Yu-wen Cheng, Ta-Fu Chen, and Ming-Jang Chiu. «From mild cognitive impairment to subjective cognitive decline: conceptual and methodological evolution». In: *Neuropsychiatric Disease and Treatment* (2017), pp. 491–498 (cit. on p. 9).

[34] Ronald C Petersen. «Mild cognitive impairment». In: *CONTINUUM: lifelong Learning in Neurology* 22.2 (2016), pp. 404–418 (cit. on p. 9).

[35] Marilyn S Albert et al. «The diagnosis of mild cognitive impairment due to Alzheimer's disease: recommendations from the National Institute on Aging-Alzheimer's Association workgroups on diagnostic guidelines for Alzheimer's disease». In: *Focus* 11.1 (2013), pp. 96–106 (cit. on p. 9).

[36] Avinash Chandra, George Dervenoulas, Marios Politis, and Alzheimer's Disease Neuroimaging Initiative. «Magnetic resonance imaging in Alzheimer's disease and mild cognitive impairment». In: *Journal of neurology* 266 (2019), pp. 1293–1302 (cit. on p. 10).

[37] Timo Kirschstein and Rüdiger Köhling. «What is the source of the EEG?» In: *Clinical EEG and neuroscience* 40.3 (2009), pp. 146–149 (cit. on p. 12).

[38] Michael X Cohen. «Where does EEG come from and what does it mean?» In: *Trends in neurosciences* 40.4 (2017), pp. 208–218 (cit. on pp. 12, 14).

[39] Katarzyna Blinowska and Piotr Durka. «Electroencephalography (eeg)». In: *Wiley encyclopedia of biomedical engineering* (2006) (cit. on pp. 13, 14).

[40] V Salai Selvam and S Shenbagadevi. «Brain tumor detection using scalp EEG with modified wavelet-ICA and multi layer feed forward neural network». In: *2011 Annual International Conference of the IEEE Engineering in Medicine and Biology Society*. IEEE. 2011, pp. 6104–6109 (cit. on p. 14).

[41] Kenneth G Jordan. «Emergency EEG and continuous EEG monitoring in acute ischemic stroke». In: *Journal of clinical neurophysiology* 21.5 (2004), pp. 341–352 (cit. on p. 14).

[42] Soheyl Noachtar and Jan Rémi. «The role of EEG in epilepsy: a critical review». In: *Epilepsy & Behavior* 15.1 (2009), pp. 22–33 (cit. on p. 14).

[43] Robert W Thatcher, Duane M North, Richard T Curtin, Rebecca A Walker, Carl J Biver, Juan F Gomez, and Andres M Salazar. «An EEG severity index of traumatic brain injury». In: *The Journal of neuropsychiatry and clinical neurosciences* 13.1 (2001), pp. 77–87 (cit. on p. 14).

[44] Bettina Platt and Gernot Riedel. «The cholinergic system, EEG and sleep». In: *Behavioural brain research* 221.2 (2011), pp. 499–504 (cit. on p. 14).

[45] Martijn Arns, C Keith Conners, and Helena C Kraemer. «A decade of EEG theta/beta ratio research in ADHD: a meta-analysis». In: *Journal of attention disorders* 17.5 (2013), pp. 374–383 (cit. on p. 14).

[46] Steven L Bressler and Mingzhou Ding. «Event-related potentials». In: *Wiley encyclopedia of biomedical engineering* (2006) (cit. on pp. 14, 15).

[47] DHR Blackwood and Walter J Muir. «Cognitive brain potentials and their application». In: *The British Journal of Psychiatry* 157.S9 (1990), pp. 96–101 (cit. on p. 14).

[48] Shravani Sur and Vinod Kumar Sinha. «Event-related potential: An overview». In: *Industrial psychiatry journal* 18.1 (2009), pp. 70–73 (cit. on p. 15).

[49] Terence W Picton and Robert F Hink. «Evoked potentials: how? what? and why?» In: *American Journal of EEG Technology* 14.1 (1974), pp. 9–44 (cit. on p. 15).

[50] J Vernon Odom, Michael Bach, Colin Barber, Mitchell Brigell, Michael F Marmor, Alma Patrizia Tormene, Graham E Holder, and Vaegan. «Visual evoked potentials standard (2004)». In: *Documenta ophthalmologica* 108 (2004), pp. 115–123 (cit. on p. 15).

[51] Srimant P Tripathy and Dennis M Levi. «On the effective number of tracked trajectories in amblyopic human vision». In: *Journal of Vision* 8.4 (2008), pp. 8–8 (cit. on p. 15).

[52] Donnell Joseph Creel. «Visually evoked potentials». In: *Handbook of clinical neurology* 160 (2019), pp. 501–522 (cit. on p. 15).

[53] Francesco Di Russo, Antıgona Martınez, Martin I Sereno, Sabrina Pitzalis, and Steven A Hillyard. «Cortical sources of the early components of the visual evoked potential». In: *Human brain mapping* 15.2 (2002), pp. 95–111 (cit. on p. 15).

[54] Michael P Philpot, Devyani Amin, and Raymond Levy. «Visual evoked potentials in Alzheimer's disease: correlations with age and severity». In: *Electroencephalography and Clinical Neurophysiology/Evoked Potentials Section* 77.5 (1990), pp. 323–329 (cit. on p. 16).

[55] Viktor K Jirsa and Hermann Haken. «Field theory of electromagnetic brain activity». In: *Physical review letters* 77.5 (1996), p. 960 (cit. on p. 17).

[56] Viktor K Jirsa and Roxana A Stefanescu. «Neural population modes capture biologically realistic large scale network dynamics». In: *Bulletin of mathematical biology* 73 (2011), pp. 325–343 (cit. on p. 17).

[57] Hugh R Wilson and Jack D Cowan. «Excitatory and inhibitory interactions in localized populations of model neurons». In: *Biophysical journal* 12.1 (1972), pp. 1–24 (cit. on p. 17).

[58] Tilo Schwalger, Moritz Deger, and Wulfram Gerstner. «Towards a theory of cortical columns: From spiking neurons to interacting neural populations of finite size». In: *PLoS computational biology* 13.4 (2017), e1005507 (cit. on p. 17).

[59] David H Hubel and Torsten N Wiesel. «Receptive fields and functional architecture of monkey striate cortex». In: *The Journal of physiology* 195.1 (1968), pp. 215–243 (cit. on p. 17).

[60] Robert A Moss, Ben P Hunter, Dhara Shah, and TL Havens. «A theory of hemispheric specialization based on cortical columns». In: *The Journal of Mind and Behavior* (2012), pp. 141–171 (cit. on p. 17).

[61] David LaBerge and Ray S Kasevich. «Neuroelectric tuning of cortical oscillations by apical dendrites in loop circuits». In: *Frontiers in Systems Neuroscience* 11 (2017), p. 37 (cit. on p. 17).

[62] Edward G Jones. «Microcolumns in the cerebral cortex». In: *Proceedings of the National Academy of Sciences* 97.10 (2000), pp. 5019–5021 (cit. on p. 17).

[63] Gustavo Deco, Viktor K Jirsa, Peter A Robinson, Michael Breakspear, and Karl Friston. «The dynamic brain: from spiking neurons to neural masses and cortical fields». In: *PLoS computational biology* 4.8 (2008), e1000092 (cit. on p. 17).

[64] Christopher J Honey, Olaf Sporns, Leila Cammoun, Xavier Gigandet, Jean-Philippe Thiran, Reto Meuli, and Patric Hagmann. «Predicting human resting-state functional connectivity from structural connectivity». In: *Proceedings of the National Academy of Sciences* 106.6 (2009), pp. 2035–2040 (cit. on p. 18).

[65] Ben H Jansen, George Zouridakis, and Michael E Brandt. «A neurophysiologically-based mathematical model of flash visual evoked potentials». In: *Biological cybernetics* 68 (1993), pp. 275–283 (cit. on p. 20).

[66] Ben H Jansen and Vincent G Rit. «Electroencephalogram and visual evoked potential generation in a mathematical model of coupled cortical columns». In: *Biological cybernetics* 73.4 (1995), pp. 357–366 (cit. on pp. 20, 21).

[67] Jukka Sarvas. «Basic mathematical and electromagnetic concepts of the biomagnetic inverse problem». In: *Physics in Medicine & Biology* 32.1 (1987), p. 11 (cit. on pp. 25, 29).

[68] Hannelore Aerts, Michael Schirner, Ben Jeurissen, Dirk Van Roost, Eric Achten, Petra Ritter, and Daniele Marinazzo. «Modeling brain dynamics in brain tumor patients using the virtual brain». In: *Eneuro* 5.3 (2018) (cit. on p. 29).

[69] Viktor K Jirsa et al. «The virtual epileptic patient: individualized whole-brain models of epilepsy spread». In: *Neuroimage* 145 (2017), pp. 377–388 (cit. on p. 29).

[70] Leon Stefanovski, Paul Triebkorn, Andreas Spiegler, Margarita-Arimatea Diaz-Cortes, Ana Solodkin, Viktor Jirsa, Anthony Randal McIntosh, Petra Ritter, and Alzheimer's Disease Neuroimaging Initiative. «Linking molecular pathways and large-scale computational modeling to assess candidate disease mechanisms and pharmacodynamics in Alzheimer's disease». In: *Frontiers in computational neuroscience* 13 (2019), p. 54 (cit. on p. 29).

[71] Salvatore Mazzeo et al. «PRedicting the EVolution of SubjectIvE Cognitive Decline to Alzheimer's Disease With machine learning: the PREVIEW study protocol». In: *BMC neurology* 23.1 (2023), p. 300 (cit. on pp. 29, 30).

[72] Alberto Arturo Vergani et al. «Event-Related Potential Markers of Subject Cognitive Decline and Mild Cognitive Impairment during a sustained visuo-attentive task». In: *bioRxiv* (2024), pp. 2024–01 (cit. on pp. 29, 30).

[73] Lorenzo Gaetano Amato et al. «Personalized modeling of Alzheimer's disease progression estimates neurodegeneration severity from EEG recordings». In: *Alzheimer's & Dementia: Diagnosis, Assessment & Disease Monitoring* 16.1 (2024), e12526 (cit. on pp. 30, 31, 33).

[74] Shani Waninger, Chris Berka, Amir Meghdadi, Marija S Karic, Kimberly Stevens, Cinthya Aguero, Tatiana Sitnikova, David H Salat, and Ajay Verma. «Event-related potentials during sustained attention and memory tasks: Utility as biomarkers for mild cognitive impairment». In: *Alzheimer's & Dementia: Diagnosis, Assessment & Disease Monitoring* 10 (2018), pp. 452–460 (cit. on p. 31).

[75] Samuel Chiquita, Ana C Rodrigues-Neves, Filipa I Baptista, Rafael Carecho, Paula I Moreira, Miguel Castelo-Branco, and António F Ambrósio. «The retina as a window or mirror of the brain changes detected in Alzheimer's disease: critical aspects to unravel». In: *Molecular neurobiology* 56 (2019), pp. 5416–5435 (cit. on p. 56).

[76] Hélène Kergoat, Marie-Jeanne Kergoat, Lisette Justino, Howard Chertkow, Alain Robillard, and Howard Bergman. «Visual retinocortical function in dementia of the Alzheimer type». In: *Gerontology* 48.4 (2002), pp. 197–203 (cit. on p. 56).

[77] Richard A Armstrong. «Alzheimer's disease and the eye». In: *Journal of Optometry* 2.3 (2009), pp. 103–111 (cit. on p. 56).

[78] Z Kubová, J Kremláček, M Vališ, J Langrová, J Szanyi, F Vıt, and M Kuba. «Visual evoked potentials to pattern, motion and cognitive stimuli in Alzheimer's disease». In: *Documenta ophthalmologica* 121 (2010), pp. 37–49 (cit. on p. 56).